Salmon Forever's 2013 Annual Report on Suspended Sediment, Peak Flows, and Trends in Elk River and Freshwater Creek, Humboldt County, California

SWRCB Agreement No. 07-508-551-0

June, 2013

Photo: South Fork Elk River at station SFM: Jun 13, 2013

Submitted to Redwood Community Action Agency

Submitted By Salmon Forever
Project Director: Jesse Noell
Author: Jack Lewis

TABLE OF CONTENTS

INTRODUCTION

This document updates data sets and summaries submitted to RCAA in Salmon Forever's June 2010 report, and presents new analyses of trends in peaks flows and sediment discharge from Elk River and Freshwater Creek. The document is best viewed electronically as it contains hyperlinks to much useful documentation. If this document is separated from the rest of the package the hyperlinks will no longer function. The package consists of water, sediment discharge, and ancillary data and analyses for HY2003 through HY2013 from four stream gaging stations on Freshwater Creek and Elk River, tributaries to Humboldt Bay, in the North Coast District. Two gaging stations in each watershed are operated using the Turbidity Threshold Sampling (TTS) system (Lewis and Eads, 2009). Gaging station locations are South Fork Elk River at Jesse Noell's house (SFM), North Fork Elk River at Kristi Wrigley's house (KRW), Freshwater Creek at Terry Roelofs' house (FTR), and Freshwater Creek at Howard Heights Bridge (HHB). Maps and aerial photos can be found in the folder Maps to roughly locate stations and cross sections. Storm flows and peaks have been extracted for 106 storm events, defined by a minimum flow of 20 cfs/mi^2 at the FTR gaging station. Suspended sediment loads were determined for storm events through hydrologic year (HY) 2008, as well as HY2011 and, for SFM and KRW, HY2013 as well. Inter-storm loads were also computed and added to storm loads to obtain annual sediment loads. Suspended sediment concentration (SSC) from nearly 6000 pumped samples have been included in the computation of storm loads. As a byproduct of load estimation, a record of SSC was produced at 10-minute intervals for all stations, from which quantiles of SSC and exceedence durations were extracted at various levels and related to salmonid stress using severity-off-ill-effects indices..

The major analytical product of this report is an evaluation of trends in storm peak flows, storm event loads, storm mean SSC, and instantaneous SSC. Multiple regression was used to relate these variables to each other and to rainfall variables, especially hourly and daily antecedent precipitation indices. Time series methods were used to account for serial autocorrelation. Trends were evaluated via scatterplots and tested by including time in the regression models.

In addition to the gaging station data, cross-sections have been surveyed at many locations on both streams, and changes in mean elevation and cross-sectional area were determined from successive surveys at each location. The previously submitted cross-section report is included in this package as a separate document, and the main results are restated here.

Watershed Descriptions

Freshwater Creek. The Freshwater Creek watershed drains into the northern end of Humboldt Bay in Northern California just north of Eureka. The Redwood and Douglas-fir forested watershed trends southeast to northwest. The watershed is mainly underlain by Franciscan, Yager and Wildcat geological formations. Portions of the northeast

watershed are composed of Franciscan melange formation. Until 2008, Pacific Lumber Company (Palco) was the major landowner in the Freshwater Creek Watershed. Since their bankruptcy, these areas have been taken over by Humboldt Redwoods Company (HRC). Salmon Forever maintains two continuous TTS monitoring stations in Freshwater Creek. Station HHB is in the lower portion of the watershed at Howard Heights bridge and the FTR station is higher on the mainstem Freshwater Creek 400 yards above Freshwater Park. The watershed area above Site FTR covers 13.2 mi^2. The watershed area draining to site HHB is 27.8 mi^2. The average suspended sediment yield from sites HHB (HY2005-2008, 2011) and FTR (HY 2003-2008, 2011) was 285 and 467 tons/mi^2, respectively.

Elk River. The Elk River Watershed drains into Humboldt Bay just south of Eureka. The watershed area is 56.1 mi^2. The Redwood and Douglas-fir forested watershed also trends northwest to southeast. The main geologic units are the Wildcat Group underlain by the Yager Formation. Palco, Green Diamond Resources Corporation (GDRC), and the BLM were the primary landowners in Elk River watershed until 2008 when Palco lands were acquired by HRC. Elk River is the largest watershed to drain into Humboldt Bay. Salmon-Forever operates two continuous TTS monitoring stations in Elk River. Site KRW is located on the North Fork Elk River 1.0 miles above the confluence of North and South Fork Elk Rivers. The watershed area above site KRW is 22.2 mi^2, of which 98% is privately managed by HRC. Site SFM is located on the South Fork Elk River approximately 0.5 miles above the confluence. The watershed area above site SFM is 19.3 mi^2 of which 50% is owned by HRC, 15% by GDRC, and 30% by BLM in the Headwaters Reserve. The average suspended sediment yield from site SFM in the years that have been analyzed to date **(**2003-2008, 2011, 2013) is 797 tons/mi^2 and from site KRW (2003-2008, 2011) is 491 tons/mi^2. Sediment yields elsewhere in this report are expressed in mton/km^2 (multiply by 2.847 to get tons/mi^2).

METHODS

Gaging Stations

All four gaging stations are operated as described in the TTS Implementation guide (Lewis and Eads, 2009) and field sampling has been undertaken in accordance with the following Standard Operating Procedures provided with this data package.

- Depth-Integrated Sampling
- Discharge Measurements
- Field Instrumentation
- Turbidity Threshold Sampling

During the period HY03-13 each gaging station had a Campbell CR10X or CR510 data logger, an ISCO Model 3700, 6700 or 6712 pumping sampler; Druck 1830 pressure transducers were standard. Turbidity sensors were suspended from a bridge-mounted or bank-mounted boom. OBS-3 turbidity sensors were used prior to HY05 at KRW and SFM, and prior to HY04 at FTR. Beginning in HY05, DTS-12 sensors were standard, but

an OBS-3 was substituted occasionally during malfunctions. The DTS-12 sensors generally produce higher quality data because they have built-in mechanical wipers that clean the optics before each reading. The DTS-12 sensors also can record water temperature as well as turbidity. If turbidity is to be analyzed as a measure of water quality, it is important to remember that these two types of sensors operate according to different principles and their output is not equivalent without adjustment (Lewis, 2007). In addition if sensors are not calibrated on a regular basis, turbidity values from the same sensor may not even be comparable. In developing relationships between turbidity and SSC, data from different sensor types are never combined without adjustment. For analyses reported in this document, turbidity values are used only to calculate SSC. Relationships between turbidity and SSC are developed for each storm event and station, so differences among sensors and long-term drift are unimportant.

Isokinetic depth-integrated samples are taken in order to calibrate the pumped samples to a cross-sectionally discharge-weighted mean SSC. However, too few samples have been collected to develop relationships. Since the load at these gaging stations is predominantly fine sediment, and the channels are relatively small, the sediment is likely to be quite well-mixed and easily extracted by a pumping sampler. Therefore the error from using SSC from pumped samples is expected to be unimportant.

Site FTR had continuous rainfall data recorded by a Campbell TR525I 5" tipping bucket rain gage in HY2003-2009. In HY2010, ISCO 8" model 674 tipping bucket rain gages were installed at all stations.

Laboratory

Samples from water years HY03-06 were processed at the Sunnybrae Sediment Laboratory in Arcata, managed by Clark Fenton. Samples from water years HY07-13 were processed at the Laboratory in Elk River, managed by Kristi Wrigley. SSC is determined by vacuum filtration through tared 1-micron glass fiber filters. Filters are oven-dried at 105º C, cooled in a dessicator, and weighed on a Precisa XB-120-A balance to the nearest 0.0001 g. Sample water weight and sediment weight is used to calculate SSC in mg/L. A subset of samples is washed through a 0.063 mm sieve prior to vacuum filtration for determination of sand content. Laboratory methods are in accordance with the Standard Operating Procedures for Laboratory SSC provided with this data package.

Budgetary and logistical constraints did not permit the timely filtering of ISCO samples in water years 2009, 2010, and 2012. The concentrations for these samples need to be adjusted for possible contamination by growth of algae. The filters have been retained so that the organics can be burned off. This work has not yet been completed. Therefore sediment loads and concentrations for those years are not included in this report. HY2013 loads and concentrations are included for stations SFM and KRW only.

Trend Detection Methodology

Trend detection is the main focus of this report. Methods used here are statistically well-established but innovative for the field of hydrology and, in the author's opinion, the most powerful available. Responses analyzed are storm event peaks, storm event loads, storm event mean SSC, and instantaneous SSC. Analysis of annual values is less revealing because of the small sample sizes and low resolution graphics. The only true control in the vicinity is Little South Fork of the Elk but recent data from that station were not available for this report. Although relative trends may be (and were) analyzed by regressing watershed responses against one another, a more insightful approach was sought.

The objective was to explain as much of the variation as possible in each response using hydrologic variables related to rainfall and runoff so that if a trend were present, its signal would not be hidden in unexplained noise. This is actually a very conventional idea, but most hydrologists have attacked the problem with simple linear regression. The main innovation here is identifying additional covariates that could reduce the unexplained variance. For storm peaks, rainfall totals and daily and hourly antecedent precipitation indexes (API) were used. For storm event loads, storm event peaks and event flow volume were used. For instantaneous concentration, instantaneous discharge and API were used. To test for trend, time was added as the final covariate and tested for significance.

Variables were selected and variable transformations determined using multiple regression diagnostic plots (Cook and Weisberg, 1994). Partial regression plots (also known as added-variable plots) show the contribution of a variable to the model after accounting for the remaining predictors. Partial residual plots (also know as component-plus-residual plots) show whether each predictor needs to be transformed to linearize its relationship to the response. Normality of residuals was evaluated using quantile-quantile plots.

For the significance test of the trend to be valid it is important that one of two conditions is satisfied: (1) the regression errors are independent and identically distributed, or (2) an appropriate model for the non-independent errors is incorporated into the regression. When observations are closely spaced in time or space, they are typically serially autocorrelated. That is, knowledge of the residual for one observation provides information about neighboring residuals. Most typically, neighboring residuals are similar in magnitude. If positively autocorrelated errors exist but are ignored, the p-value of the time term will be underestimated. The underestimation can be very great, depending on the degree of autocorrelation. For storm event data, autocorrelation may exist, but it is not usually very large. For sediment concentration data collected using TTS, there can be many samples per storm event, and serial autocorrelation is usually very great. For ten-minute data such as turbidity, or SSC estimated from turbidity, serial autocorrelation is extreme.

For this project, serial autocorrelation was evaluated for regression models using the Durbin-Watson statistic (Durbin and Watson, 1971), calculated in the *lmtest* package

(Achim et al., 2002) of the *R statistical environment* (R Development Core Team, 2008). When serial autocorrelation was detected, ARMA (autoregressive moving average) models (Box and Jenkins, 1970) were incorporated into the regression using the *gls* (generalized least squares) function in the R package *nlme* (Pinheiro et al. 2007). Appropriate ARMA models were identified by evaluating autocorrelation (ACF) and partial autocorrelation (PACF) residual plots (Shumway, 1988) and selecting the one that minimized Akaike's Information Criterion (AIC) (Sakamoto et al., 1986). The adequacy of the selected ARMA model was evaluated by inspecting autocorrelation and partial autocorrelation plots of the normalized residuals. In all but one case autoregressive (AR) models without moving average components were found adequate to describe the autocorrelation.

Tests for trend are incomplete without examination of scatterplots. Tests for linear trends are misleading when the trends are not linear. If a trend is not linear it should not be tested with a linear term. Sometimes a trend can be broken into approximately linear periods that can be tested separately. Such an analysis permits a more accurate characterization of trends but the tests for significance must be interpreted very conservatively. When we let the data define the hypothesis to be tested, the p-values cannot be interpreted literally. There are many periods that could be tested; testing periods with the most pronounced trends is, in effect, testing all possible periods that could be tested. For example, in a 10-year period there are 45 ways to choose a starting and ending year. If all periods were independent and the rejection level were set at p=0.05, then in 45 tests of random data, the probability of at least one significant test is 0.90. The 45 tests are not independent so an accurate calculation of experiment-wise error-rate is difficult; the important thing to remember is that letting the data determine the hypothesis inflates Type I errors (the probability of rejecting a hypothesis that is in fact true), so the p-values must be interpreted as relative measures rather than absolute probabilities. In the search for short-term trends, I considered p-values between 0.005 and 0.05 as suggestive of a weak trend but not definitive.

To help identify time trends in scatterplots, curves were fitted by *loess* (locally weighted scatterplot smoothing) (Cleveland et al., 1992), a non-parametric fitting technique that produces continuous functions of arbitrary shape. (The name comes from locally weighted smoothing spline). At each point *x*, a polynomial fit is made using points in a neighbourhood of *x*, weighted by their distance from *x*. The size of the neighborhood is controlled by a parameter that in effect regulates the smoothness of the fit. Unless stated otherwise, the smoothing parameter, or *span*, was set at 0.8 in the plots shown in this report. In inspecting these plots it is important to remember that the "wiggliness" of the loess curves depends strongly on the smoothing parameter. The curve does not necessarily pass through the mean of points in a given year, because its position is influenced by surrounding years.

Relative trends, comparing one location to another, were investigated by computing simple linear regressions relating the storm event responses (peaks, loads, or mean SSC) at two gaging stations, and examining the time sequence of residuals. The storm start date (number of days since an arbitrary origin) was added to the regressions to test for

trend. Although these models only can show relative trends, they sometimes have a greater ability to detect trends than other models because more of the variability is explained. Relationships between KRW and SFM, and between HHB and FTR are the least variable. And they can help to confirm and complement models based on rainfall and flow. Responses were transformed using logarithms or square roots if necessary to linearize the relationships or equalize the variance throughout the range of observations. Comparisons were made between (1) KRW and SFM, (2) KRW and FTR, (3) SFM and FTR, and (4) HHB and FTR. All watersheds were compared to FTR because it seemed to generally be the watershed with the steadiest responses.

This section has been an overview of the methodology common to all the trend tests in this report. Methods specific to each analysis are described in the Analysis and Results section.

PRODUCTS

The primary data products of this report are water and sediment discharge for both storm events and water years, as well as a 10-minute record of flow and SSC for each gaging station.

The Data

FILE FORMATS

Data files in a TTS database consist of plain ASCII text only. These files have various extensions but are simply text files that can be viewed with any text editor or easily be imported into any spreadsheet, database, or statistical program. See File Formats.doc for a description of the standard files in a TTS database.

PLOTTING THE DATA

The stage and turbidity data in the appended/corrected **.flo** data files can be plotted using the TTS Adjuster program, which can be started from the preceding hyperlink. When prompted for a starting month, enter August. On the initial screen, click on the "Browse" button, and specify the "Data" directory of this package as the TTS Home directory. After selecting a station, file, and start/end dates or dumps, click correspondingly on "Read Dates" or "Read Dumps" to view a plot. Zooming in and out can be accomplished by dragging the mouse. Scatterplots of SSC and turbidity for the displayed time window can be obtained by clicking on the"Scatterplot" button. Additional instructions are found in the TTS Adjuster manual, which is also available via the programs' help button.

Discharge Rating Curves

Stage/discharge rating curves applied at the gaging stations are shown in Figures 1-4. As more measurements are collected each year, rating curves are occasionally recomputed. Rating curves have been updated at all stations but KRW during the period of study. However, there have been no large shifts detected in any of the rating curves. Cross-section surveys (at SA5, NA2, and HH2) indicate aggradation of 0.43 to 0.81 ft during the monitoring period at stations, SFM, KRW, and HHB; so it is possible that with more discharge measurements, shifts might have been detected. Discharge measurements are plotted using symbols that identify the water year of the measurement. Some of the outlier measurements were not included in estimation of any of the rating curves. At SFM, three measurements taken on Dec. 20, 24, and 28, 2005 lie below the general scatter and these were excluded from calculation of the rating curves based on a comparison with storm peak flows at KRW during this period. Stations FTR and KRW each have an outlier point in HY2005 that was thought to result from measurement error, and these too were excluded from calculation of their rating curves. Rating curves generally take the form of 2nd order polynomials. In many cases, separate low-flow and high-flow polynomial segments are required to fit all the data. All past and current rating equations are stored in **.sdr** files in the TTS database.

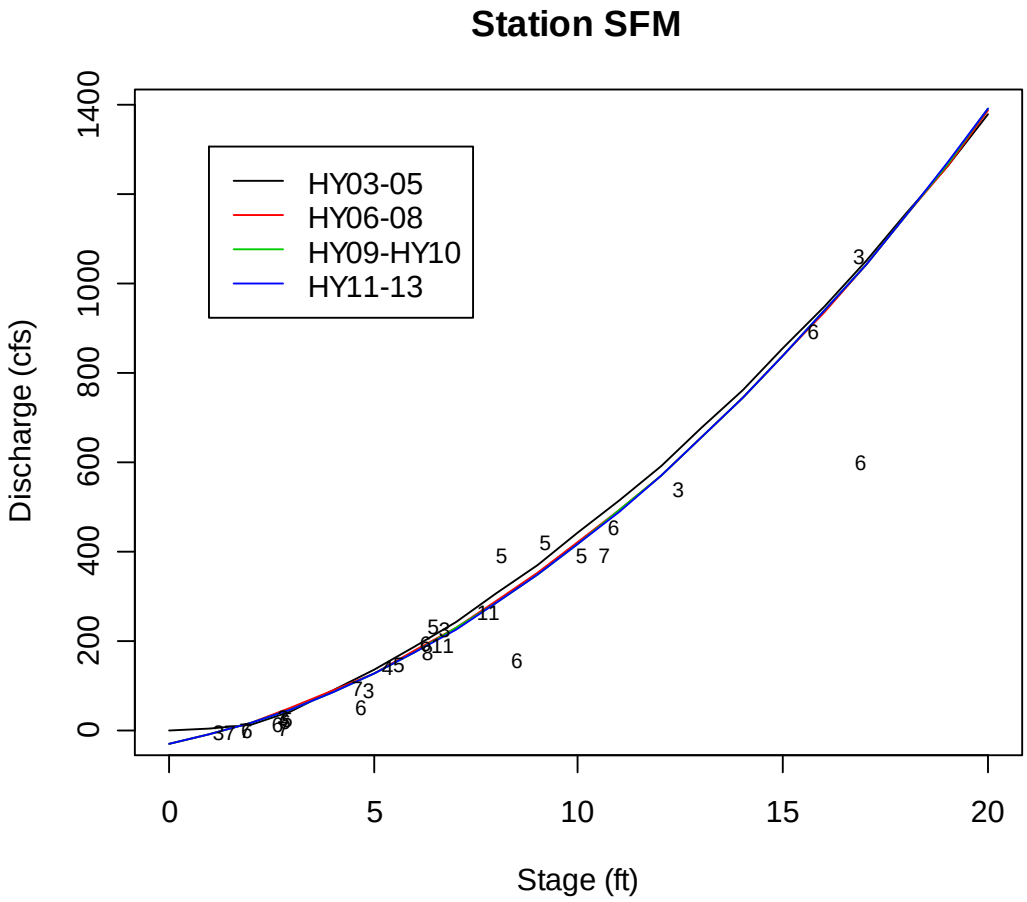

Figure 1. Discharge measurements and rating curves applied at station SFM.

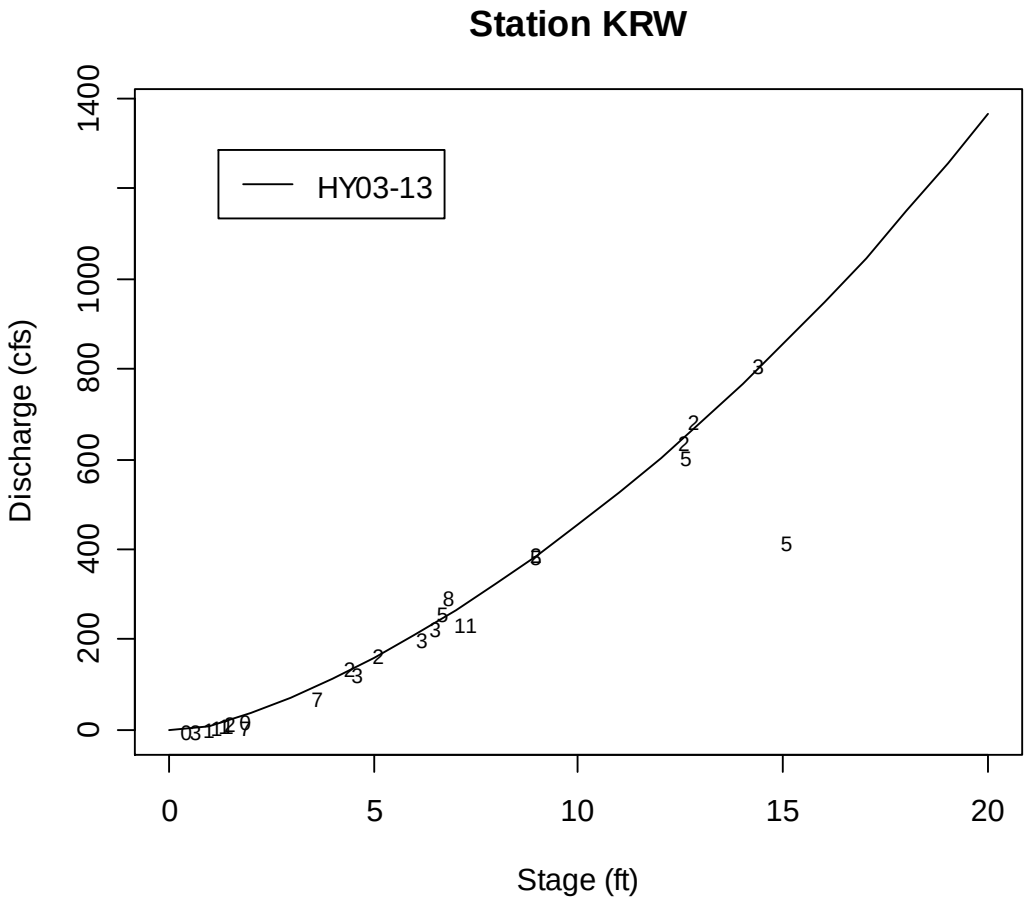

Figure 2. Discharge measurements and rating curves applied at station KRW.

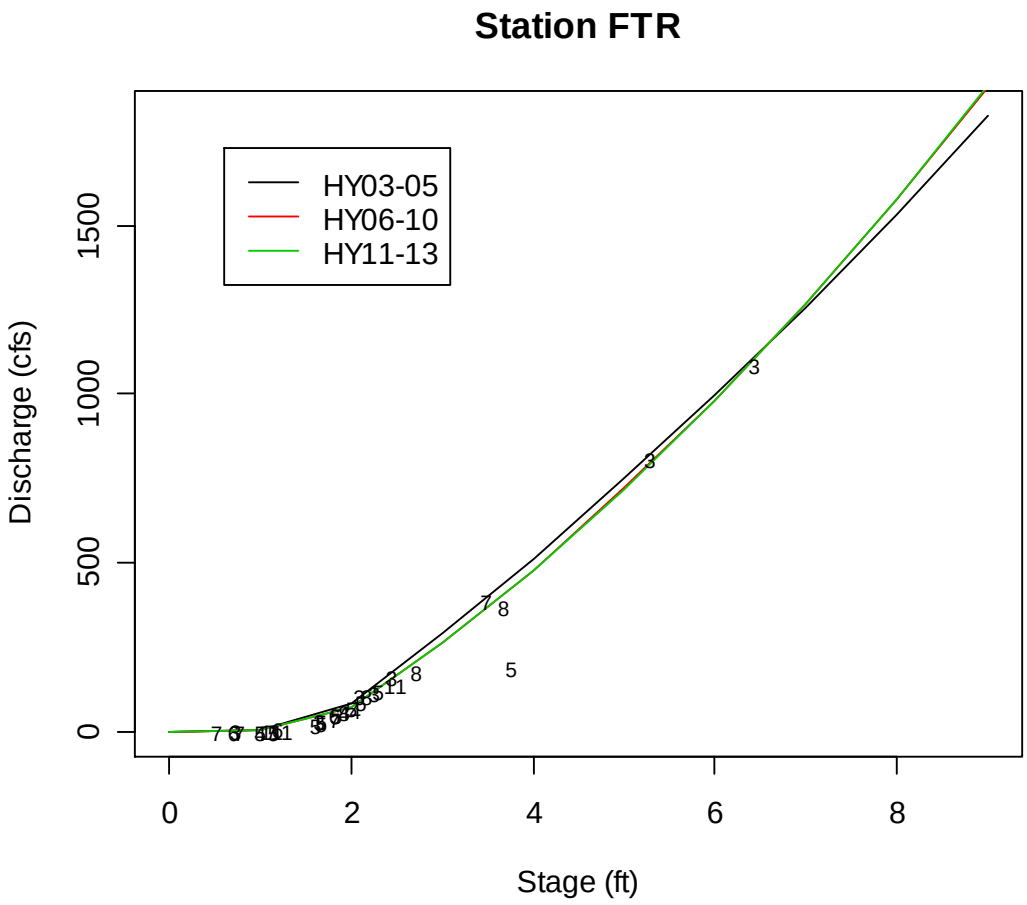

Figure 3. Discharge measurements and rating curves applied at station FTR.

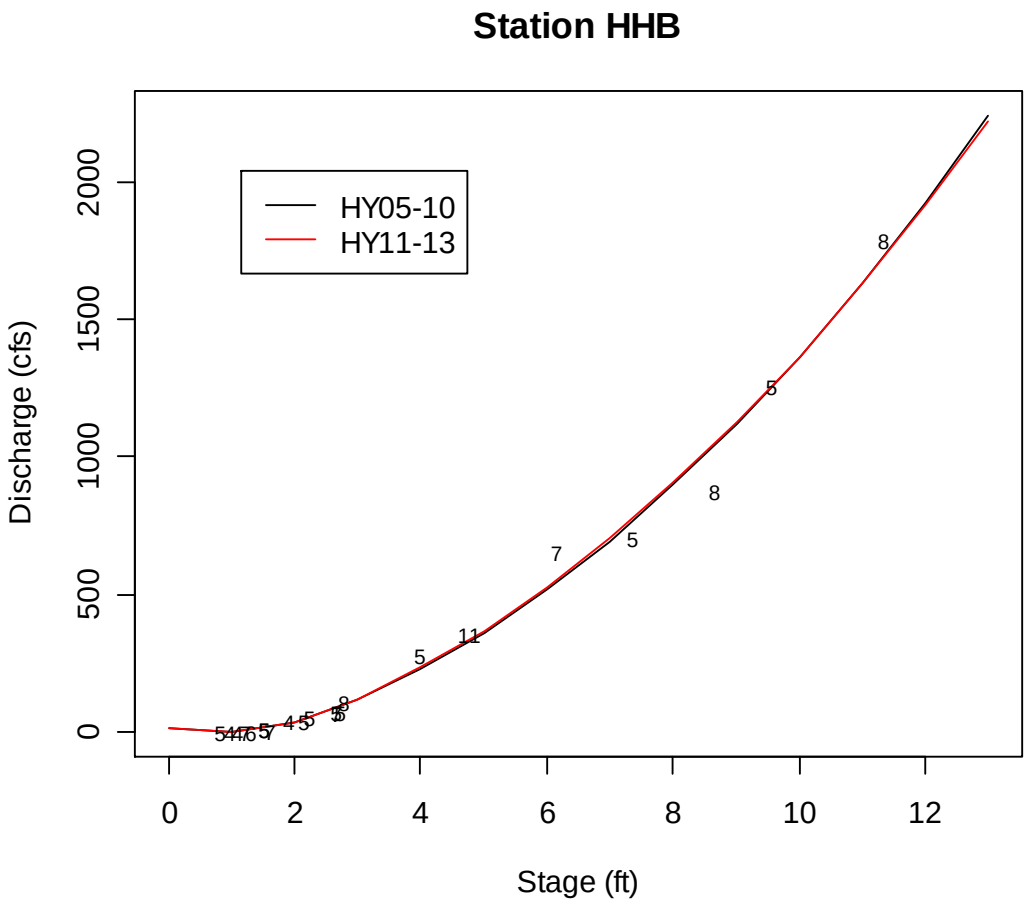

Figure 4. Discharge measurements and rating curves applied at station HHB.

Annual Maximum Peak Discharges

Figure 5 shows the annual maximum instantaneous peak discharges for HY2003-2013. The nearby JBW gaging station operated by Randy Klein at Brookwood Bridge on Jacoby Creek, also draining to Humboldt Bay, is included in the figure for comparison. Discharge was not measured at HHB before 2005, and the peak for JBW in HY2013 has not yet been determined. The years of maximum peak discharge are 2003 and 2011, depending on the watershed. The four highest annual peaks were all measured at station FTR, and during the wettest years, its unit area peak substantially exceeds that measured downstream at HHB. HY2009 was by far the driest year of the monitoring period for all stations.

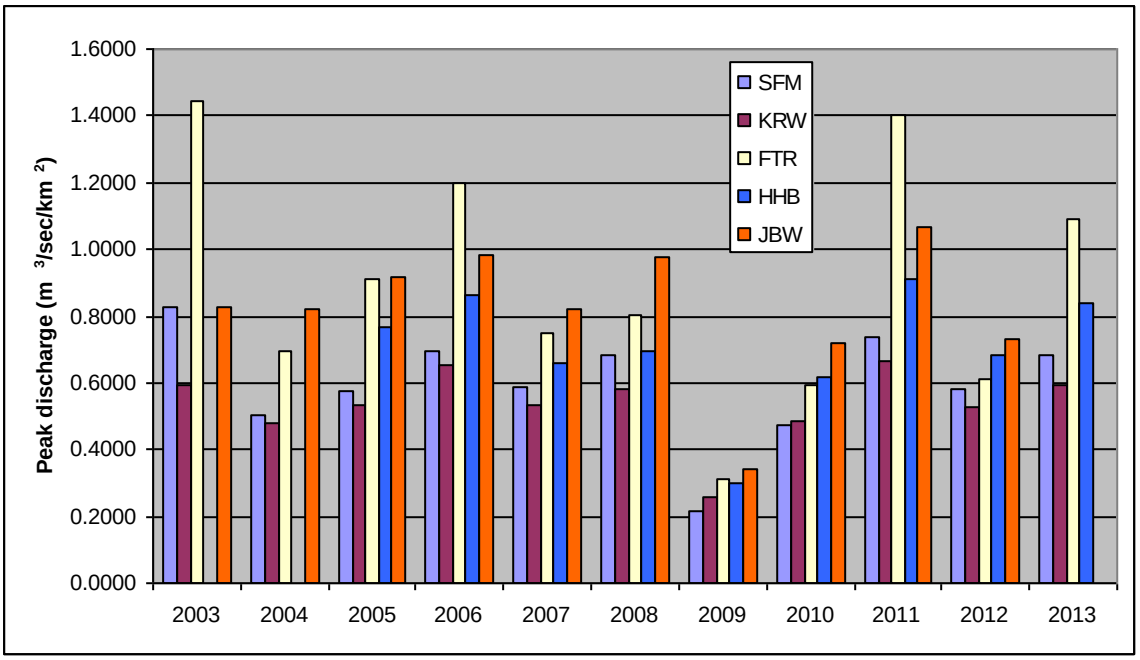

Figure 5. Annual peak discharges per unit area at Humboldt Bay gaging stations

Annual Suspended Sediment Loads

Annual suspended sediment yields are displayed in Figure 6, again alongside Jacoby Creek for comparison. In addition to the missing data that was identified in the annual peaks data, bars are missing for HY09, HY10, and HY12 for all the Salmon-Forever Station, as well as HY13 for the Freshwater gages. These data sets have not been finalized yet, as discussed under Laboratory Operations. Based on yields at station JBW and peak flows at all stations, the missing Salmon-Forever years (HY09, 10, and 12) are among the four least hydrologically consequential years of the monitoring period. Among the remaining years, station SFM has had the highest unit sediment yields every year. Rankings are fairly uniform, with KRW usually in distant second place, followed closely by FTR, and HHB trailing behind. In all years except HY06, JBW has very similar unit yields as KRW and FTR.

The unit sediment yield from the old-growth Little South Fork watershed in the Headwaters Reserve averaged 13.8 mton/km^2 from 2004 to 2011 (Sullivan, 2013), less than the smallest yield from JBW in Figure 6. That value is dwarfed by the mean unit yield at SFM of 280 mton/km^2 from SFM (2003 to 2013). If the Headwaters Reserve, which comprises 30% of the SFM watershed, has unit yield between 1 and 5 times that of Little South Fork then the average unit yield from industry-managed lands in the SFM watershed is between 370 and 395 mton/km^2, exceeding the maximum yield measured during the monitoring period from stations KRW, FTR, HHB, and JBW.

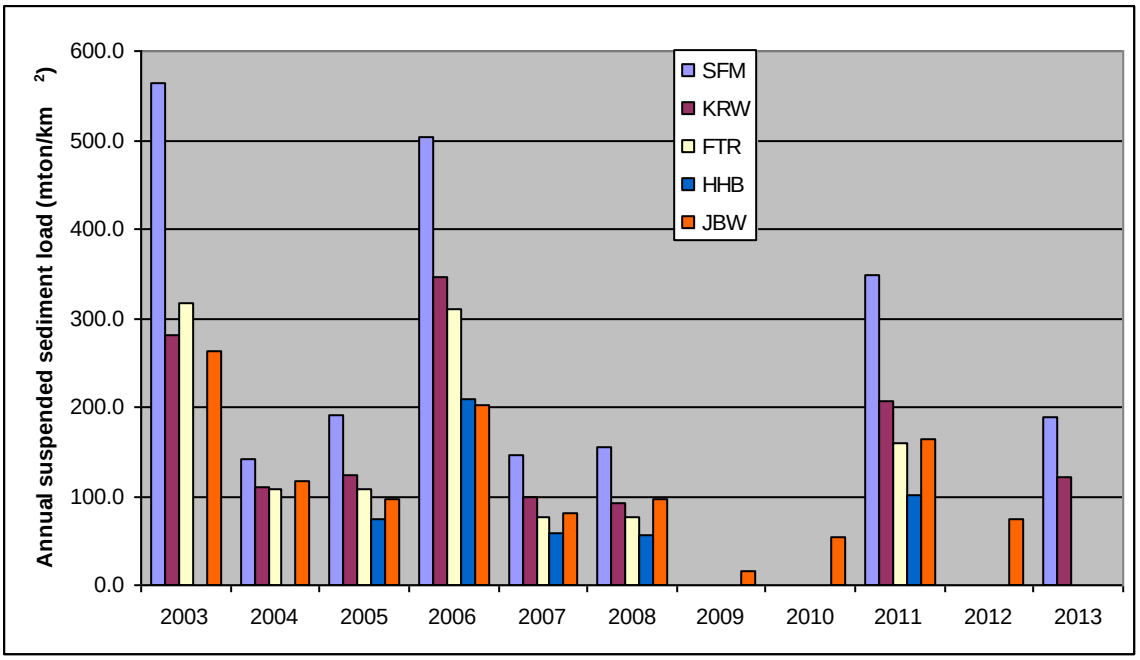

Figure 6. Annual suspended sediment loads per unit area at Humboldt Bay gaging stations

Severity of Ill Effects

When estimating storm event loads from TTS data, a 10-minute record of SSC is generated using storm-specific relationships of SSC with turbidity from pumped samples. When there are problems with turbidity, storm estimates are developed using time-interpolation or, on rare occasion, from discharge-sediment rating curves. Interstorm periods are estimated using annual relationships, and the storm and interstorm data sets are merged to produce unusually accurate and detailed records of SSC. From these records, maximum annual durations of continuous exposure at different levels of SSC have been extracted and are shown in Table 1. These are not annual exceedence times, they are the maximum durations of periods for which exposure was continually above the specified values. The exposure data were then used to compute severity-of-stress indexes developed by Newcombe and MacDonald (1991) and Newcombe and Jensen (1996), which relate the duration and concentration of sediment exposure to stress on aquatic organisms. The latter publication includes 4 models of severity for different groupings of salmonid life stages. The annual maximum continuous exposure hours and severity of ill-effect scores are shown below in Table 2 and are also provided in SEV scores.xls. For KRW HY13, exposures at 55 and 20 mg/L are omitted from severity Tables 2 because the durations (Table 1) were excessive given the relatively mild winter; there were problems estimating low concentrations that year at KRW because the turbidity probe output declined, resulting in a lack of TTS samples. In general, our estimation of SSC during baseline conditions is less reliable than during storm periods because TTS predominantly collects samples during storm periods when SSC is elevated and interstorm values must be estimated from annual relationships.

Table 1. Maximum continuous hours above various SSC levels.

	Maximum Continuous Hours above specified SSC					
Site/HY	2981	1097	403	148	55	20
SFM/03	6.2	41.5	62.7	174.2	303.8	1157.2
KRW/03	0	18.3	46	68.2	154.8	547.3
FTR/03	0	13	39	51.7	63.7	245.5
SFM/04	0	4.7	29.5	80.7	110	252.2
KRW/04	0	2	27.3	64.7	91.3	459.3
FTR/04	0	2.5	15.2	48.7	65.8	135
SFM/05	0	8.3	27.7	83.7	215.8	569
KRW/05	0	8.7	18	35.3	163	718
FTR/05	0	4.2	15.7	28	58.2	164.2
HHB/05	0	1.3	9.3	29.8	49.3	206
SFM/06	0.3	22.8	111.2	480	1067.8	1362.7
KRW/06	0	8.8	37	77	337	1311.3
FTR/06	3	9.2	17.7	45.3	135.2	478.5
HHB/06	0	4.8	18.8	57	154.7	448
SFM/07	0	13.8	39.8	76.7	255.2	518.2
KRW/07	0	2	22.8	46.2	257.3	391
FTR/07	0	1	15.2	29.8	61.3	257.5
HHB/07	0	0	11.2	29.7	101.5	273.8
SFM/08	0	15	37.3	114.8	255.5	1349.2
KRW/08	0	3.2	16.7	38	211.5	389
FTR/08	0	3.7	10.2	22.2	89.5	253.2
HHB/08	0	2.5	9	23.7	56.5	264.3
SFM/11	4.2	15	78.2	274	1131.3	1414.7
KRW/11	0	9.2	25.8	67.5	131.2	894.5
FTR/11	2.3	9	20	33.5	59.7	547.7
HHB/11	0	2.7	17	35.3	68.7	286.5
SFM/13	0	13.8	49.2	81.3	180.2	453.7
KRW/13	0	7.7	19.5	74.2	258*	2923*

* Unreliable

Table 2. Severity-of-ill-effects (SEV) scores for four models based on SSC durations (Model 1: adult and juvenile salmonids combined; Model 2: adult salmonids only; Model 3: juvenile salmonids only; Model 4: salmonid eggs and larvae). Color codes are defined below table.

Model 1	Suspended Sediment Concentration (mg/L)					
Site/HY	2981	1097	403	148	55	20
SFM/03	8.1	8.5	8	7.9	7.5	7.6
KRW/03	0	8	7.8	7.3	7.1	7.1
FTR/03	0	7.8	7.7	7.1	6.5	6.6
SFM/04	0	7.2	7.5	7.4	6.9	6.6
KRW/04	0	6.7	7.5	7.3	6.8	7
FTR/04	0	6.8	7.1	7.1	6.6	6.3
SFM/05	0	7.5	7.5	7.4	7.3	7.1
KRW/05	0	7.5	7.2	6.9	7.1	7.3
FTR/05	0	7.1	7.2	6.8	6.5	6.4
HHB/05	0	6.4	6.8	6.8	6.4	6.5
SFM/06	6.3	8.1	8.4	8.5	8.3	7.7
KRW/06	0	7.6	7.7	7.4	7.6	7.6
FTR/06	7.6	7.6	7.2	7.1	7	7
HHB/06	0	7.2	7.3	7.2	7.1	7
SFM/07	0	7.8	7.7	7.4	7.4	7.1
KRW/07	0	6.7	7.4	7.1	7.4	6.9
FTR/07	0	6.2	7.1	6.8	6.5	6.6
HHB/07	0	0	7	6.8	6.8	6.7
SFM/08	0	7.9	7.7	7.6	7.4	7.6
KRW/08	0	6.9	7.2	7	7.3	6.9
FTR/08	0	7	6.9	6.6	6.8	6.6
HHB/08	0	6.8	6.8	6.7	6.5	6.7
SFM/11	7.8	7.9	8.1	8.2	8.3	7.7
KRW/11	0	7.6	7.5	7.3	7	7.4
FTR/11	7.5	7.6	7.3	6.9	6.5	7.1
HHB/11	0	6.8	7.2	6.9	6.6	6.7
SFM/13	0	7.8	7.9	7.4	7.2	7
KRW/13	0	7.5	7.3	7.4		

Model 2	Suspended Sediment Concentration (mg/L)					
Site/HY	2981	1097	403	148	55	20
SFM/03	8.6	8.8	8.2	7.9	7.4	7.3
KRW/03	0	8.4	8	7.5	7.1	7
FTR/03	0	8.2	8	7.3	6.7	6.6
SFM/04	0	7.7	7.8	7.6	7	6.6
KRW/04	0	7.3	7.8	7.5	6.9	6.9
FTR/04	0	7.4	7.5	7.3	6.7	6.3
SFM/05	0	8	7.8	7.6	7.3	7
KRW/05	0	8	7.6	7.2	7.1	7.1
FTR/05	0	7.7	7.5	7.1	6.7	6.4
HHB/05	0	7.1	7.3	7.1	6.6	6.5
SFM/06	7.2	8.5	8.5	8.4	8	7.4
KRW/06	0	8	7.9	7.5	7.5	7.4
FTR/06	8.3	8	7.6	7.3	7.1	6.9
HHB/06	0	7.7	7.6	7.4	7.1	6.9
SFM/07	0	8.2	8	7.5	7.4	6.9
KRW/07	0	7.3	7.7	7.3	7.4	6.8
FTR/07	0	7	7.5	7.1	6.7	6.6
HHB/07	0	0	7.4	7.1	6.9	6.6
SFM/08	0	8.3	7.9	7.7	7.4	7.4
KRW/08	0	7.5	7.6	7.2	7.3	6.8
FTR/08	0	7.6	7.3	6.9	6.9	6.6
HHB/08	0	7.4	7.3	7	6.6	6.6
SFM/11	8.4	8.3	8.3	8.1	8.1	7.4
KRW/11	0	8	7.8	7.5	7	7.2
FTR/11	8.1	8	7.6	7.1	6.7	7
HHB/11	0	7.4	7.6	7.2	6.7	6.6
SFM/13	0	8.2	8.1	7.6	7.2	6.9
KRW/13	0	7.9	7.6	7.5		

SEV8-8.9 SEV9-9.9 SEV10-10.9 SEV11-11.9 SEV≥12

Table 2 (continued). Severity-of-ill-effects (SEV) scores for four models based on SSC durations (Model 1: adult and juvenile salmonids combined; Model 2: adult salmonids only; Model 3: juvenile salmonids only; Model 4: salmonid eggs and larvae).

Model 3	Suspended Sediment Concentration (mg/L)					
Site/HY	2981	1097	403	148	55	20
SFM/03	7.7	8.3	7.9	7.9	7.6	7.8
KRW/03	0	7.8	7.7	7.3	7.1	7.3
FTR/03	0	7.5	7.6	7.1	6.5	6.7
SFM/04	0	6.8	7.4	7.4	6.9	6.8
KRW/04	0	6.2	7.3	7.2	6.8	7.2
FTR/04	0	6.4	6.9	7	6.5	6.3
SFM/05	0	7.2	7.3	7.4	7.4	7.3
KRW/05	0	7.2	7	6.8	7.2	7.5
FTR/05	0	6.7	6.9	6.6	6.4	6.5
HHB/05	0	5.9	6.6	6.7	6.3	6.6
SFM/06	5.7	7.9	8.3	8.6	8.5	7.9
KRW/06	0	7.3	7.6	7.4	7.7	7.9
FTR/06	7.2	7.3	7	7	7	7.2
HHB/06	0	6.8	7.1	7.1	7.1	7.2
SFM/07	0	7.6	7.6	7.3	7.5	7.3
KRW/07	0	6.2	7.2	7	7.5	7.1
FTR/07	0	5.7	6.9	6.7	6.5	6.8
HHB/07	0	0	6.7	6.7	6.8	6.8
SFM/08	0	7.6	7.6	7.6	7.5	7.9
KRW/08	0	6.5	7	6.9	7.4	7.1
FTR/08	0	6.6	6.6	6.5	6.8	6.8
HHB/08	0	6.4	6.6	6.5	6.4	6.8
SFM/11	7.4	7.6	8.1	8.2	8.5	8
KRW/11	0	7.3	7.3	7.3	7	7.6
FTR/11	7	7.3	7.1	6.8	6.5	7.3
HHB/11	0	6.4	7	6.8	6.6	6.8
SFM/13	0	7.6	7.8	7.4	7.2	7.2
KRW/13	0	7.2	7.1	7.3		

Model 4	Suspended Sediment Concentration (mg/L)					
Site/HY	2981	1097	403	148	55	20
SFM/03	8.2	10	10.1	11	11.3	12.4
KRW/03	0	9.1	9.8	9.9	10.5	11.6
FTR/03	0	8.7	9.6	9.6	9.5	10.7
SFM/04	0	7.6	9.3	10.1	10.1	10.7
KRW/04	0	6.7	9.2	9.9	9.9	11.4
FTR/04	0	6.9	8.6	9.6	9.6	10
SFM/05	0	8.2	9.3	10.1	10.9	11.6
KRW/05	0	8.3	8.8	9.2	10.6	11.9
FTR/05	0	7.5	8.6	9	9.4	10.3
HHB/05	0	6.2	8.1	9	9.3	10.5
SFM/06	5	9.4	10.8	12.1	12.6	12.6
KRW/06	0	8.3	9.6	10.1	11.4	12.5
FTR/06	7.4	8.4	8.8	9.5	10.4	11.4
HHB/06	0	7.7	8.8	9.7	10.5	11.4
SFM/07	0	8.8	9.6	10.1	11.1	11.5
KRW/07	0	6.7	9	9.5	11.1	11.2
FTR/07	0	5.9	8.6	9	9.5	10.8
HHB/07	0	0	8.3	9	10.1	10.8
SFM/08	0	8.9	9.6	10.5	11.1	12.6
KRW/08	0	7.2	8.7	9.3	10.9	11.2
FTR/08	0	7.4	8.2	8.7	9.9	10.7
HHB/08	0	6.9	8	8.8	9.4	10.8
SFM/11	7.8	8.9	10.4	11.4	12.7	12.6
KRW/11	0	8.4	9.2	9.9	10.3	12.1
FTR/11	7.2	8.3	8.9	9.1	9.5	11.6
HHB/13	0	7	8.7	9.2	9.6	10.9
SFM/13	0	8.8	9.9	10.1	10.7	11.4
KRW/08	0	8.2	8.9	10		

SEV8-8.9 SEV9-9.9 SEV10-10.9 SEV11-11.9 SEV≥12

Severity of ill-effects (SEV) scores correspond to impact levels as follows:

1. SEV 8-8.9 (major physiological stress),
2. SEV 9-9.9 (reduced growth rate and density, delayed hatching),

3. SEV 10-10.9 (10-20% mortality),
4. SEV 11-11.9 (20-40% mortality), and
5. SEV≥12 (40-60% mortality).

Applying Newcombe and Jensen's Model 2 for adult salmonids we find a maximum severity of 8.8 for our period of record occurring at SFM in HY03. A severity of 9 is defined as a sublethal effect associated with reduced growth and population density. A severity of 8 was exceeded at SFM in all years except HY04. The same severity of 8 was exceeded in 4 of 8 years at KRW, 3 of 7 years at FTR, and 0 of 5 years at HHB. Newcombe and Jensen (1996) defined severity 8 as indicating major physiological stress with long-term reductions in feeding success.

Newcombe and Jensen's Model 3 indicates that conditions for juvenile salmonids are not as stressful as for adults. Annual maximum severity scores for juveniles varied from 7.4 to 8.6 at SFM, 7.3 to 8.5 at KRW, 6.8 to 7.6 at FTR, and 6.7 to 7.2 at HHB.

Suspended sediment's harshest effects are on the most sensitive but abundant life stages: salmonid eggs and larvae. A maximum SEV score of 12.7 occurred at SFM in HY11. Severities above 12 occurred in 4 of 8 years at SFM and in 2 of 8 years at KRW. A severity of 12 is defined as a lethal effect with 40-60% mortality and a severity of 13 is associated with 60-80% mortality. A severity of 11, associated with 20-40% mortality, was exceeded at SFM in all years but HY04, and at KRW in all years except possibly 2013, but was only exceeded at the Freshwater stations in HY06 and at FTR in HY11 Model 4 SEV scores above 10 occurred every year at all stations, suggesting 0-20% mortality, increased predation, and moderate to severe habitat degradation.

We did not have SSC data for the specific size fractions to which the models are said to pertain, therefore our calculations are based on the total SSC without regard to grain size. Our SSC data exclude some particles finer than 1μ but may include sizes coarser than 250μ; the former bias is more important at low concentrations and the latter more important at high concentrations. It might be possible to improve these calculations using our sand fraction data, since our sand break at 63μ is not far from the 75μ break used to define the upper limit of particle sizes for models 3 and 4. Adjusting the concentrations would be subject to significant errors, however, because there are no strong relationships between sand fraction and either total SSC or discharge. See Sand Fraction Plots.doc for data on sand fractions of SSC samples.

Cross Section Changes

A report of cross-section changes was submitted to RCAA in March 2013. That report is included with this package and should be referred to for a detailed description of results. The main results are repeated in the following paragraphs and summarized by cross-section in Tables 3 and 4, which were not in the first report. In Freshwater Creek, 12 cross-sections have been surveyed at least twice since 1999. In the lower Elk River, 10 cross-sections on the main-stem, 14 on the North Fork, and 10 on the South Fork have been measured at least twice since 2001. Areal and elevational changes in cross-section

have been computed for the longest transect common to all surveys of a given cross-section, here called the *common survey area*. In addition elevation changes have been computed for the portion of the transect on the channel bed between the bottom of the banks.

While degradation has been measured on occasion at a few cross-sections in the Elk River (notably just below the confluence of the North and South Forks), all reach averages are either stable or aggrading. The North and South Forks are filling at a faster rate than the main-stem. The weighted average rate of infill in the South Fork has been 9.19 ft^2/yr or 0.051 ft yr^{-1} of deposition on the streambed between the bottom of the banks (Table 3). The weighted average rate of infill in the North Fork has been 6.54 ft^2yr^{-1}, with aggradation of 0.095 ft yr^{-1} between the bottom of the banks (Table 3). The main-stem Elk has been filling at a weighted average rate of 5.39 ft^2yr^{-1}, with relatively minor aggradation of 0.022 ft yr^{-1} between the bottom of the banks. Rates of aggradation between 2007 and 2011 are lower than for the decade as a whole. Some of the greatest rates of aggradation occurred in the North Fork below station KRW between 2002 and 2006.

In Freshwater Creek at Howard Heights Bridge (HH2), the only Salmon-Forever site with surveys spanning at least 10 years, aggradation rates for the decade from 1999-2010 were similar to average rates in the Elk River. In the Freshwater reaches with surveys spanning 6-7 years, average infill rates over the period ending in 2010 are near zero. Significant changes have occurred at individual cross-sections (FTR1, FTR7, and GGB) in particular years (Table 4), but the only evidence of long-term (decadal) change in Freshwater Creek is from HH2 and Army Corps of Engineer cross-section 5 (ACOE-5). Excluding the ACOE-5 cross-section, the weighted average rate of infill in Freshwater Creek has been 2.20 ft^2yr^{-1}, with aggradation of 0.031 ft yr^{-1} between the bottom of the banks. At ACOE-5, 1 km downstream from the Clete Isbel reach, measurements spanning 36 years suggest an average infill rate of about 11 ft^2yr^{-1}, but changes at ACOE-5 in the last decade are as yet unknown.

In summary, aggradation in lower Elk River has continued in the past decade and is widespread at typical rates of up to 1 foot (and in some places more) per decade. Infill is greater in the North and South Forks than in the main stem. It's not as clear what is currently happening in Freshwater Creek because of the relative sparseness of surveys, but many cross-sections seem to be stable, and average watershed-wide rates of infill since 1999 appear to be 30-50% of those in the Elk River.

Table 3. Elk River Cross Section Changes, Common Survey Area, and Channel Bed Between Bottom of Banks

Elk River			Total Change				Mean Annual Change		
Cross Section	First Survey	Latest Survey	Common Area	Common Elev	Bottom Elev	Years Spanned	Common Area	Common Elev	Bottom Elev
Mainstem			($ft^{2)}$	(ft)	(ft)		(ft^2/yr)	(ft/yr)	(ft/yr)
MBR1	2007	2011	1.7	0.02	-0.16	4	0.42	0.005	-0.041
MBR2	2007	2011	-1.8	-0.04	-0.19	4	-0.44	-0.009	-0.048
MBR3	2007	2011	15.9	0.22	0.11	4	3.98	0.054	0.027
MSX1	2010	2011	17.5	0.53	0.88	1	17.53	0.531	0.876
MLW2	2004	2011	39.9	0.51	0.53	7	5.70	0.073	0.076
MLW3	2004	2011	73.6	0.82	0.50	7	10.52	0.117	0.071
MA4	2002	2011	56.1	0.50	0.50	9	6.24	0.056	0.055
MA3	2002	2011	52.8	0.43	0.38	9	5.87	0.048	0.043
MA2	2002	2011	98.5	0.90	1.73	9	10.94	0.099	0.192
MA1	2001	2011	-9.0	-0.10	-2.86	10	-0.90	-0.010	-0.286
Totals and Reach Means			345.3	3.79	1.41	64	**5.40**	**0.059**	**0.022**
North Fork									
NC5	2001	2011	29.2	0.39	0.89	10	2.92	0.039	0.089
NC4	2001	2011	135.7	1.86	1.57	10	13.57	0.186	0.157
NC3	2001	2011	59.3	0.81	0.49	10	5.93	0.081	0.049
NC2	2001	2011	3.1	0.04	1.95	10	0.31	0.004	0.195
NC1	2001	2011	57.6	0.73	0.28	10	5.76	0.073	0.028
NSK1	2007	2011	-10.5	-0.28	-0.61	4	-2.62	-0.071	-0.153
NSK2	2007	2011	17.7	0.16	0.10	4	4.42	0.041	0.024
NSK3	2007	2011	25.1	0.24	0.19	4	6.26	0.059	0.047
NA6	2006	2011	27.9	0.29	0.17	5	5.58	0.059	0.034
NA5	2002	2006	20.8	0.29	0.04	4	5.21	0.072	0.010
NA3	2001	2011	79.9	0.94	1.09	10	7.99	0.094	0.109
NA2a	2006	2011	33.0	0.26	0.52	5	6.60	0.052	0.103
NA2	2001	2011	88.9	0.93	1.32	10	8.89	0.093	0.132
NA1	2001	2011	125.4	1.26	2.03	10	12.54	0.126	0.203
Totals and Reach Means			693.2	7.9	10.02	106	**6.54**	**0.075**	**0.095**
South Fork									
SB1	2001	2011	107.7	1.13	0.49	10	10.77	0.113	0.049
SB2	2002	2011	75.5	0.81	0.86	9	8.38	0.089	0.096
SB3	2001	2011	87.8	0.87	0.76	10	8.78	0.087	0.076
SB4	2001	2002	-17.6	-0.20	0.10	1	-17.56	-0.200	0.104
SA6	2007	2011	2.0	0.03	0.29	4	0.50	0.009	0.073
SA5	2001	2011	77.1	1.05	0.63	10	7.71	0.105	0.063
SA4	2001	2011	102.9	0.76	0.44	10	10.29	0.076	0.044
SA3	2001	2011	124.2	0.93	-0.22	10	12.42	0.093	-0.022
SA2	2001	2002	57.9	0.30	0.16	1	57.89	0.305	0.156
SA1	2001	2011	71.8	1.14	0.30	10	7.18	0.114	0.030
Totals and Reach Means			689.4	6.8	3.82	75	**9.19**	**0.091**	**0.051**

Table 4. Freshwater Creek Cross Section Changes, Common Surveyed Area, and Channel Bed Between Bottom of Banks

Freshwater Creek			Total Change				Mean Annual Change		
Cross Section	First Survey	Latest Survey	Common Area ($ft^{2)}$	Common Elev (ft)	Bottom Elev (ft)	Years Spanned	Common Area (ft^2/yr)	Common Elev (ft/yr)	Bottom Elev (ft/yr)
HH2	1999	2010	77.4	0.80	0.80	11	7.04	0.073	0.073
HH1	1999	2000	0.1	0.14	0.23	1	0.14	0.137	0.228
CI1	2004	2009	9.7	0.21	0.18	5	1.94	0.043	0.037
CI2	2004	2010	1.6	0.02	0.03	6	0.26	0.003	0.005
CI3	2004	2010	-7.7	-0.09	-0.23	6	-1.28	-0.015	-0.039
CI4	2004	2010	1.7	0.03	-0.04	6	0.29	0.004	-0.006
GGB	2003	2004	-28.6	-0.22	-0.65	1	-28.6	-0.224	-0.652
GGU	2003	2010	13.5	0.19	0.27	7	1.93	0.027	0.039
PC1	2003	2010	-5.2	-0.13	-0.21	7	-0.74	-0.019	-0.030
FTR1	1999	2005	31.6	0.58	0.77	6	5.26	0.096	0.129
FTR5	2002	2005	7.2	0.14	0.17	3	2.38	0.046	0.057
FTR7	2002	2005	22.6	0.34	0.61	3	7.52	0.114	0.202
Totals and Reach Means			152.2	1.98	1.94	62	**2.20**	**0.032**	**0.031**

TREND ANALYSES AND RESULTS

Models for Storm Peak Flow using Antecedent Precipitation

Trends in storm peak flow were investigated by modeling peak flows as a function of rainfall variables and looking for a trend that was not explained by rainfall. These models permit trend testing for each station independently of one another, but they aren't as powerful as the models in the previous section at identifying trends because the covariates do not explain as much variance in the response. The response variable in these models is the 6-hr peak flow or its logarithm. The 6-hr peak flow is the mean flow for the maximum 6-hours of flow during a storm event; it was found to be slightly more predictable than the more variable instantaneous peak. Models for the logarithm of the response exhibited somewhat more normally distributed residuals than models for the untransformed response, but with 4-8% lower explained variance.

Rainfall variables considered for modeling the peak flows were the 6, 12, 18, and 24-hour totals (T6, T12, T18, T24) at station FTR prior to the instantaneous peak, as well as an array of daily and hourly antecedent precipitation indexes (API), based on a geometric series of half-lives, shown in Table 5. API is computed as

$$\mathrm{API}_{k,i} = k\,\mathrm{API}_{k,i-1} + P_i \qquad (1)$$

where $\mathrm{API}_{k,i}$ is the API with decay coefficient k for period i. The daily API variables were based on rainfall from the Eureka National Weather Service Station in Eureka, California. These were found to be better predictors than corresponding variables based on rainfall recorded at the FTR gaging station. For hourly and finer resolution rainfall, data from station FTR was used. The daily API based on the Eureka rainfall through the

calendar day preceding each rainfall peak was further decayed at an hourly rate equivalent to its daily decay rate for the number of hours, *n*, between midnight and the time of the peak, and augmented by the FTR rainfall, P_n, recorded during those *n* hours. Mathematically, the API for a peak occurring at hour *n* on day *i* is computed as

$$API_{k,i,n} = k^{n/24} API_{k,i-1} + P_n \quad (1)$$

Variables were screened using all-possible-subsets regression up to a maximum of 5 variables. The model with the lowest value of Akaike's Information Criterion (AIC) was selected. Trend was tested by adding storm sequence number as an additional variable. Trend was significant only for station HHB (Table 6). Bear in mind that this test is for a linear trend. Trends can be visualized by looking at loess curves fitted to time sequences of residuals from the rainfall models (Figures 7-10). There is very little indication of a trend at any of the stations except HHB, whose residuals rose somewhat in the latter half of the record. By taking antilogs of the annual residual means, we can estimate that the 6-hr peaks in 2012 and 2013 averaged about 25% higher than those in 2005 and 2006 for given antecedent rainfall conditions. This result of course assumes that the discharge rating curves are accurate and stable. The outlier at the bottom of each plot is the event that occurred on 10/24/2011. This is the only October event in the study period. Antecedent conditions were very dry at the time but an unusually large amount (3") of rainfall fell in the 12 hours leading up to the peak. This increased even the slowest decaying API variable to a value comparable to that of some winter storms following dry periods, suggesting that excluding recent rainfall from slow-decaying API variables might improve prediction for some events. However, I did test lagged API variables and, in general they did not improve these models.

Table 5. API variables considered in the peak flow models

API variable	Period	Decay rate	Half-life		API Variable	Period	Decay rate	Half-life
D61	day	0.6125	1.41 d		H61	hour	0.6125	1.41 h
D71	day	0.7071	2.00 d		H71	hour	0.7071	2.00 h
D78	day	0.7827	2.83 d		H78	hour	0.7827	2.83 h
D84	day	0.8409	4.00 d		H84	hour	0.8409	4.00 h
D88	day	0.8847	5.66 d		H88	hour	0.8847	5.66 h
D92	day	0.9170	8.00 d		H92	hour	0.9170	8.00 h
D94	day	0.9406	11.31 d		H94	hour	0.9406	11.31 h
D96	day	0.9576	16.0 d		H96	hour	0.9576	16.0 h
D97	day	0.9698	22.6 d		H97	hour	0.9698	22.6 h
D98	day	0.9786	32.0 d		H98	hour	0.9786	32.0 h

Table 6. Best models for predicting 6-hr peak flow from rainfall

Station	log-transformed response	Variables in best model up to size 5					Adjusted R^2	trend p-value
SFM	no	T12	H88	H94	D61	D98	0.561	0.376
SFM	yes	T12	H84	H98	D61	H98	0.482	0.689
KRW	no	T12	H61	H78	H94	D61	0.507	0.973
KRW	yes	T12	H61	H78	H92	D61	0.458	0.845
FTR	no	T18	H71	H78	H84	D88	0.581	0.374
FTR	yes	T6	T12	H78	D61		0.519	0.657
HHB	no	T12	H92	H98	D71		0.462	0.014
HHB	yes	T12	H94	H98	D71		0.426	0.011

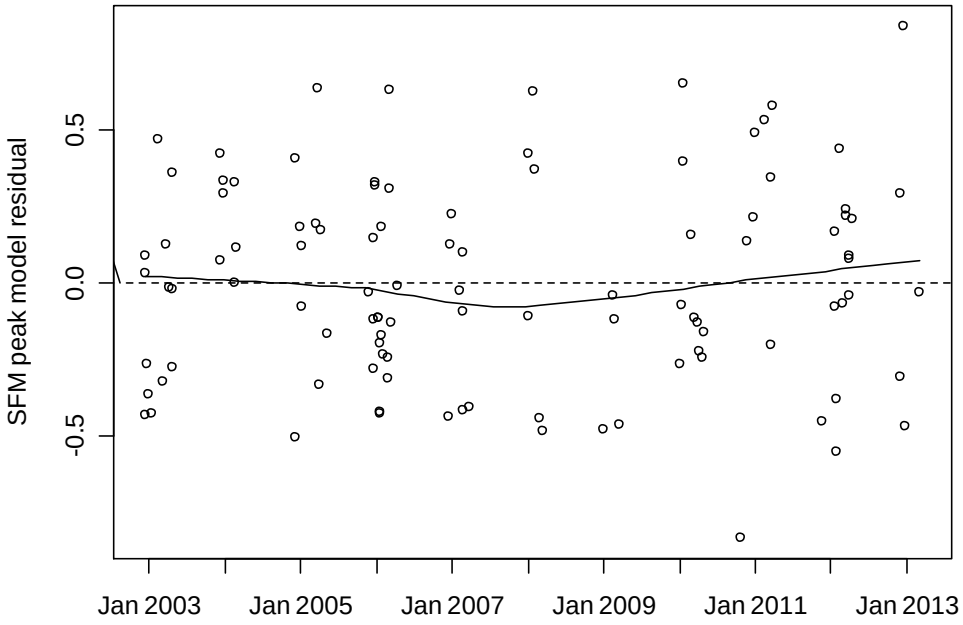

Figure 7. Residual from rainfall model for untransformed 6-hr peak at SFM

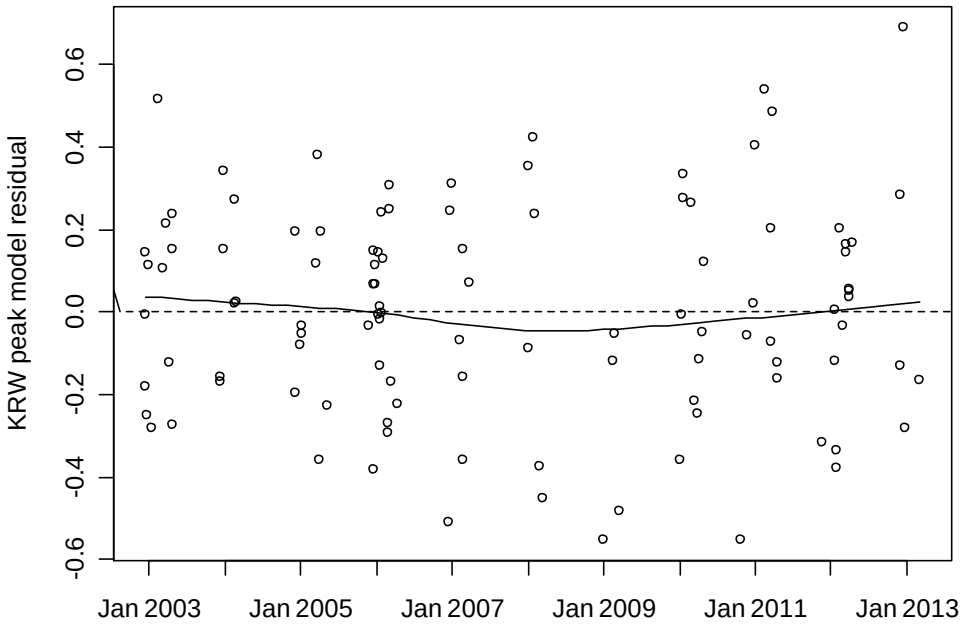

Figure 8. Residual from rainfall model for untransformed 6-hr peak at KRW

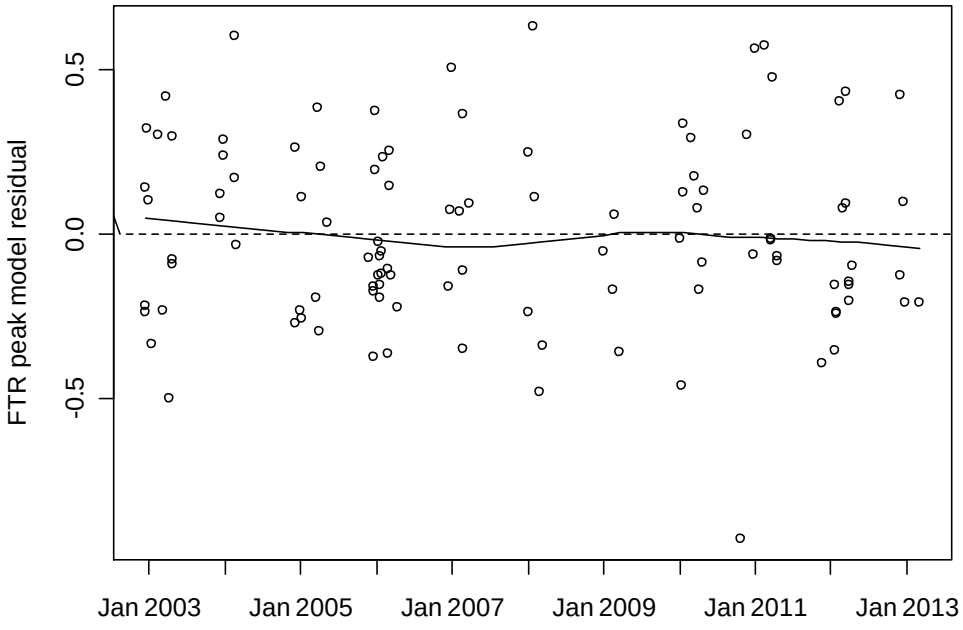

Figure 9. Residual from rainfall model for untransformed 6-hr peak at FTR

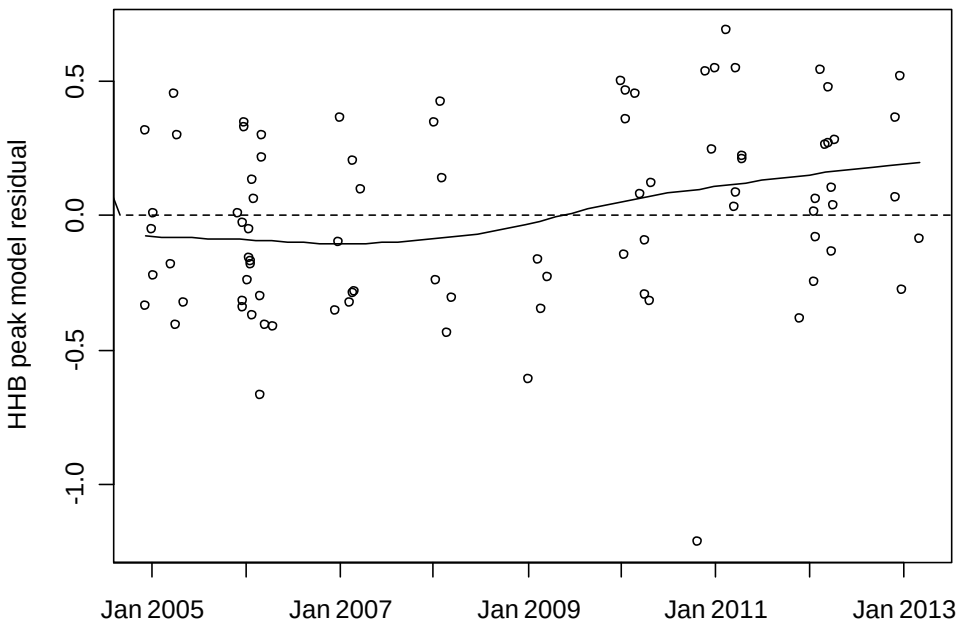

Figure 10. Residual from rainfall model for untransformed 6-hr peak at HHB

Relative Trends in Storm Peak Flow

The response variable in these models is again the 6-hr peak flow, which was found to be slightly more strongly related than the more variable instantaneous peaks. Coefficients of determination for the relative trend models varied from 0.75 to 0.93, explaining more variance than the rainfall/peak models, which had R^2 from 0.43 to 0.58. Figures 11-14 show the regressions and residuals trends. Peaks at KRW increased relative to SFM and FTR during 2003-2006 ($p < 0.001$) but the trends did not persist in subsequent years. HHB peaks increased very significantly relative to FTR from 2007-2013. Other trends are weak or non-existent (Table 7).

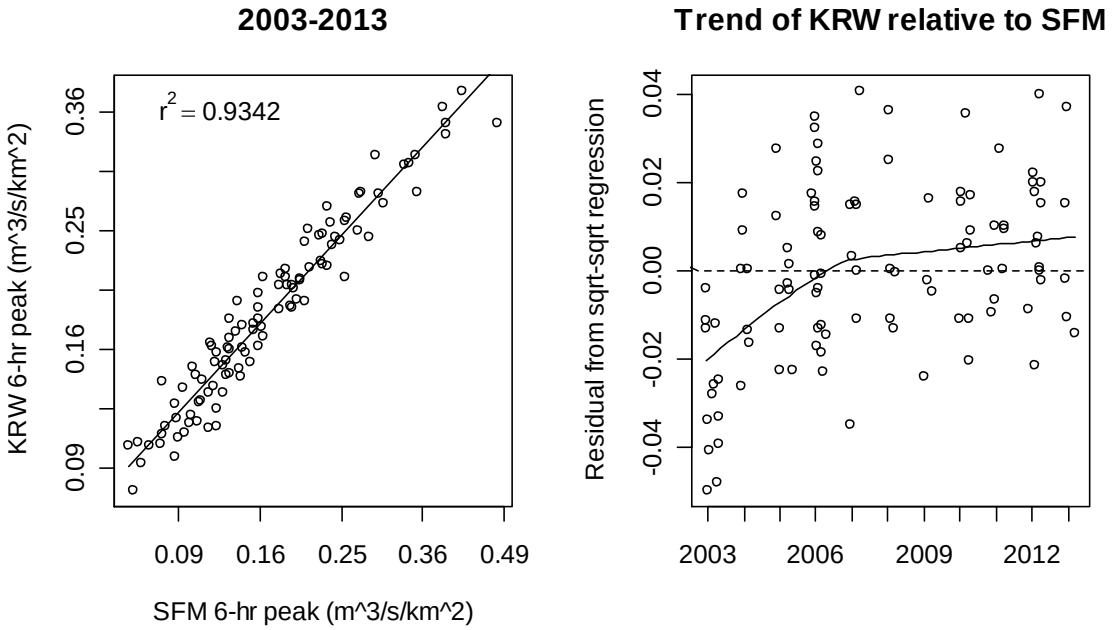

Figure 11. Trend analysis of 6-hr peak at KRW relative to SFM. Both variables were transformed by square roots.

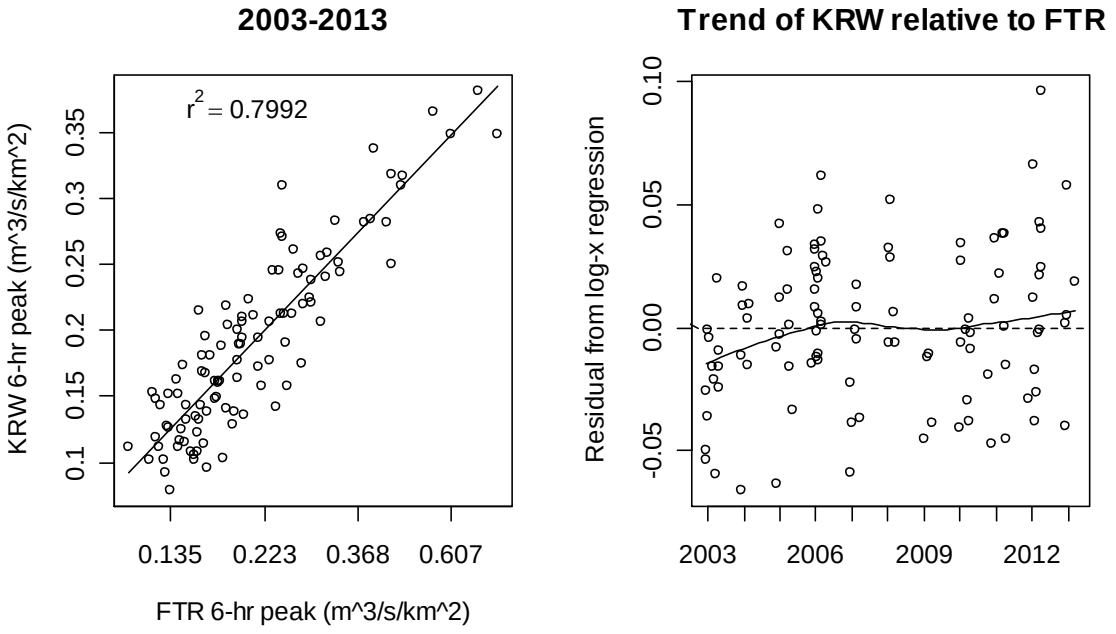

Figure 12. Trend analysis of 6-hr peak at KRW relative to FTR. The peak at only FTR was transformed by logarithms.

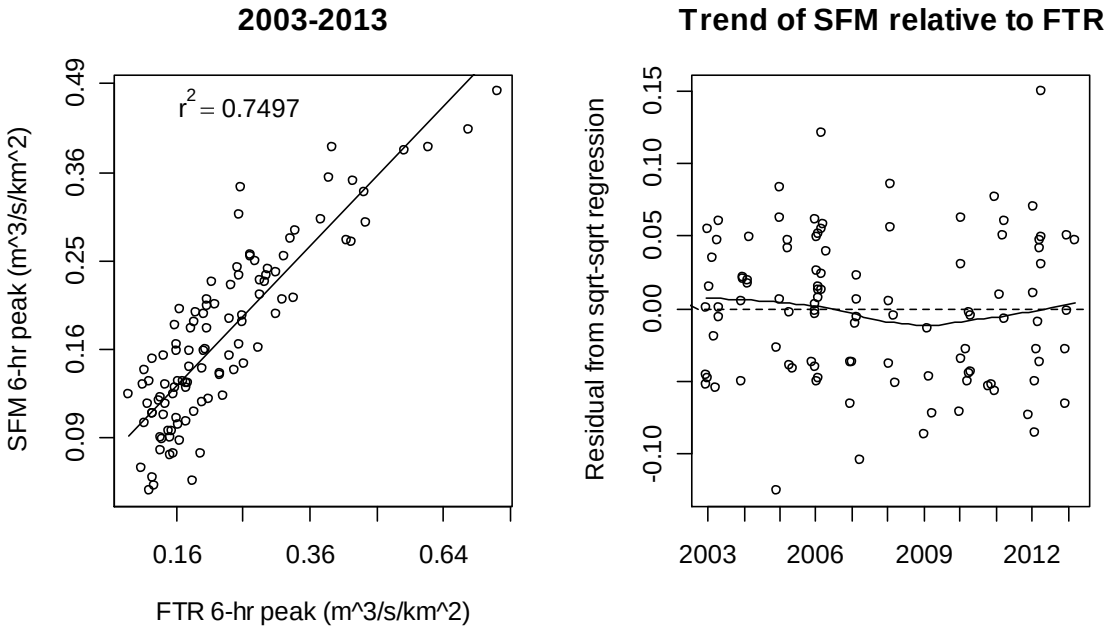

Figure 13. Trend analysis of 6-hr peak at SFM relative to FTR. Both variables were transformed by square roots.

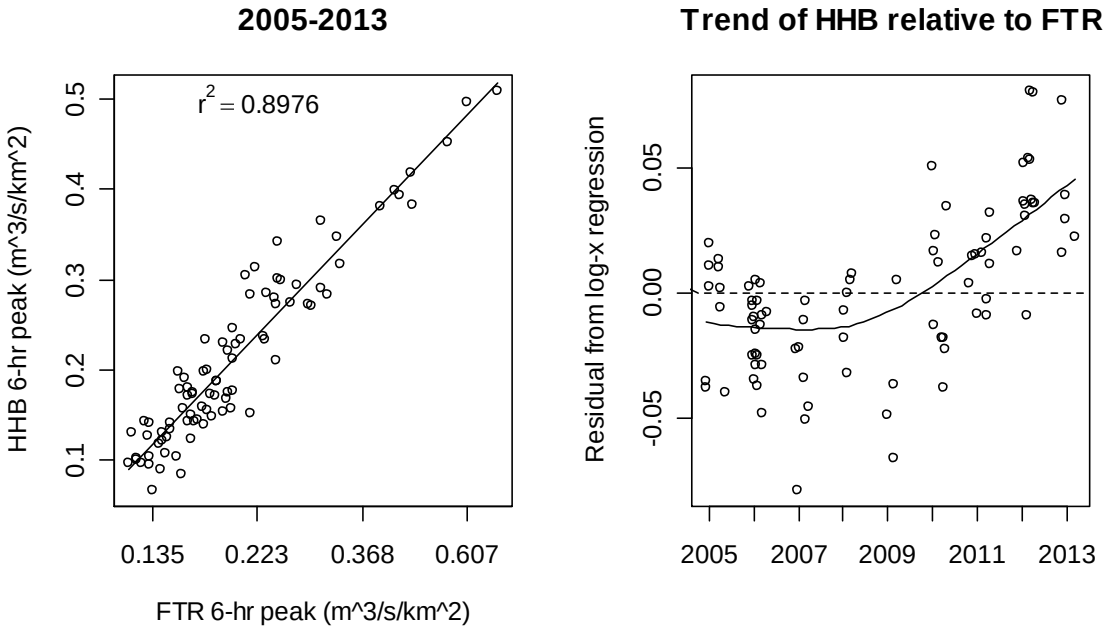

Figure 14. Trend analysis of 6-hr peak at HHB relative to FTR. The peak at FTR was transformed by logarithms.

Table 7. Summary of relative trends in storm event 6-hr mean peak flow

Y variable	X variable	Years	Trend?	R^2	Error model	Trend p-value
$KRW^{0.5}$	$SFM^{0.5}$	2003-2013	nonlinear	0.9342	none	no test
		2003-2006	increasing	0.9157	AR(1)	0.0009
		2006-2013	flat	0.9515	IID	0.6183
KRW	log(FTR)	2003-2013	flattish	0.7992	AR(1)	0.1403
		2003-2006	increasing	0.8157	IID	8.5E-05
		2007-2013	flat	0.8081	AR(1)	0.1604
$SFM^{0.5}$	$FTR^{0.5}$	2003-2013	flat	0.7497	IID	0.687
		2009-2013	slight rise	0.7115	IID	0.0412
HHB	log(FTR)	2005-2013	nonlinear	0.8976	none	no test
		2005-2007	slight fall	0.9526	IID	0.0070
		2007-2013	increasing	0.8755	IID	5.0E-10

Of the trends identified in this section, only the increase at HHB relative to FTR is supported by the earlier analysis of peak flow based on rainfall. That may simply be a result of the greater power of this analysis, which was able to explain more of the variability. The trends shown in this section could result from real changes in peak flow or they could result from changes in the relationship between stage and discharge at one or more gaging stations. If infill occurs at a gaging station, the stage is likely to be higher for a given discharge. But unless the stage/discharge rating equation is altered to account for the change, the computed flows will appear to increase as a result of the aggradation. This possibility is considered in the Discussion section.

Models for SSC using Antecedent Precipitation

The technique used in this section is a bivariate extension of a standard hydrological tool: the sediment rating curve is classically a log-log regression of suspended sediment concentration on discharge. But the influences on sediment concentration are too complex to be predicted well by a single variable such as discharge. For example sediment rating curves very typically exhibit clockwise hysteresis during storm events, (Figure 15), which is to say that the concentrations are greater during the rising limb of the event than at identical concentrations during the falling limb. Hysteresis is usually not as obvious as that shown in Figure 15 because most data sets combine a very few samples from a large number of storm events. Including one or more additional predictors has the potential to greatly increase the proportion of explained variance, making it easier to discern management-related trends in the remaining unexplained variance. Explanations for hysteresis include supply and depletion of transportable sediment, and surface erosion caused by rainfall. In either case, the recession of the hydrograph is nearly always accompanied by cessation of rainfall or at least a significant reduction in rainfall intensity. This suggests that some measure of rainfall might serve as an effective covariate in a bivariate sediment rating curve model. For example, adding an hourly API with a decay coefficient of 0.80 (H80) to the model removes most of the hysteresis from the January 4-6 storm (Figure 16).

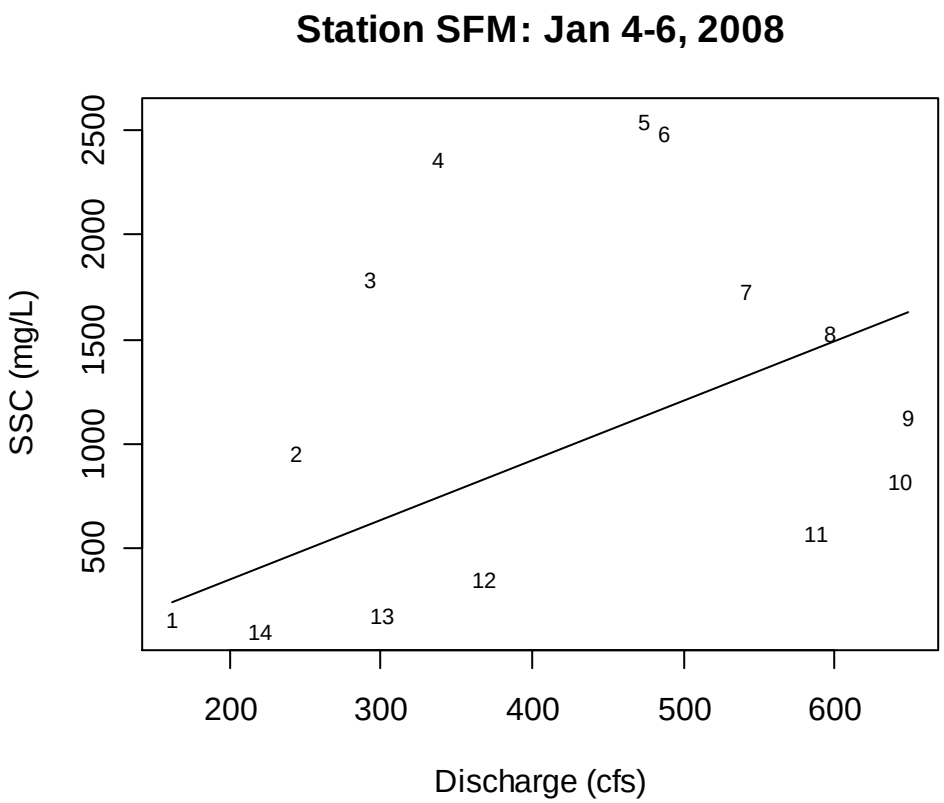

Figure 15. Typical sediment discharge rating curve from a storm event at station SFM exhibiting clockwise hysteresis. Symbols indicate the sequence of samples.

I computed hourly API values for various decay rates, based on the tipping bucket rainfall data recorded at station FTR and fit models to the set of all SSC samples collected from 2003-2013 at each gaging station. At station SFM, the API that most improved the model used a decay coefficient of 0.82, and it performed best when transformed by the square root. Together, discharge and API explained 70% of the variance in the logarithm of SSC at SFM (Figure 17), and 81 to 83% at the other gaging stations (Table 8; Figures 19, 21, and 23).

The sequence of residuals from the bivariate rating curve model for SFM shows a dip from HY2006 to HY2008 followed by a return and overshoot of the overall mean by 2013 (Figure 18). Since the log response was modelled, percentage departures from the mean SSC for a given flow and rainfall condition can be computed based on the antilog of the mean residual in a given year. The mean SSC for a given condition in 2008 lies 54% below the overall mean, while those for 2011 and 2013 lie 15% and 35%, respectively, above the mean. (As mentioned in the methods section, the loess curve is influenced by neighboring years, so it does not pass precisely through the means).

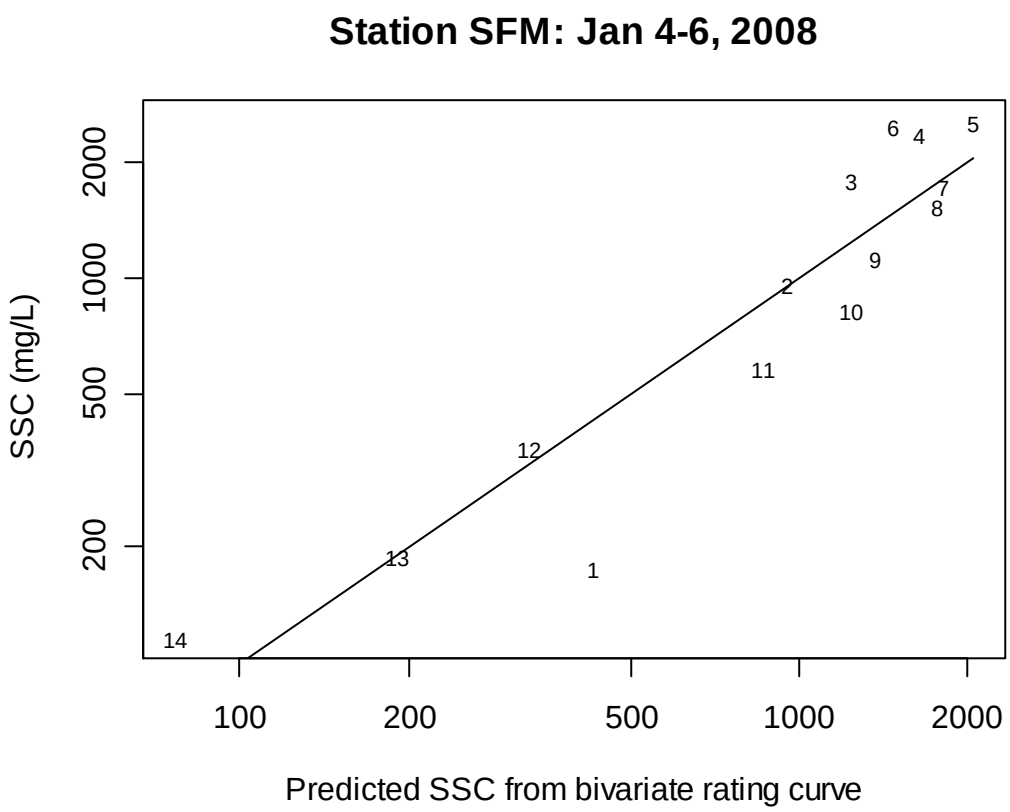

Figure 16. Observed versus predicted SSC from bivariate regression model predicting log(SSC) as a linear function of log(discharge) and hourly API (H80).

Table 8. Best bivariate models for log(SSC) and test for overall linear trend.

Station	Years	Discharge variable	API variable	Adjusted R^2	Error model	trend p-value
SFM	2003-2013	log(Q)	$H82^{0.5}$	0.6956	AR(4)	0.8960
KRW	2003-2013	log(Q)	$H84^{0.5}$	0.8169	AR(2)	0.5703
FTR	2003-2011	$Q^{0.35}$	$H86^{0.70}$	0.8101	AR(3)	0.8013
HHB	2005-2008	$Q^{0.20}$	$H85^{0.67}$	0.8305	AR(1)	0.0813

AR = denotes an autogressive process of order n.

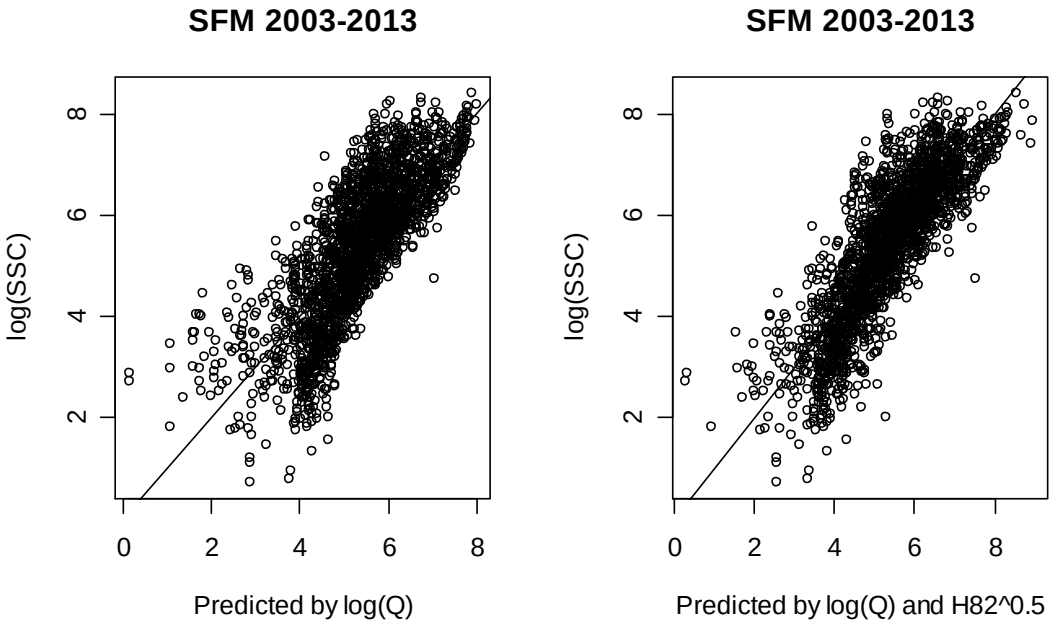

Figure 17. Observed versus predicted SSC from bivariate regression models predicting log(SSC) at station SFM as a linear function of (1) log(discharge) and (2) log(discharge) and hourly API ($H82^{0.5}$). Adding API to the model increased the adjusted R^2 from 0.625 to 0.696.

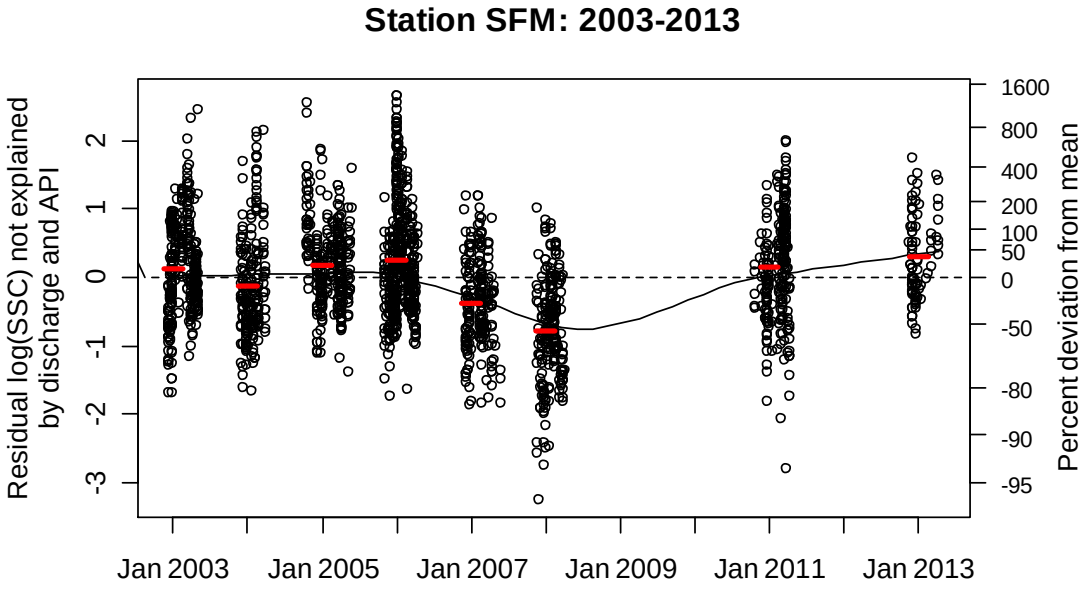

Figure 18. Sequence of residuals from bivariate regression model predicting log(SSC) at station SFM as a linear function of log(discharge) and hourly API ($H82^{0.5}$). Curve is fit by loess, with smoothing parameter = 0.67. Red bars show annual means.

Because TTS sampling can be quite frequent during storms, the sample concentrations are not independent. Rating curve residuals exhibit very significant serial autocorrelation. Hypothesis testing without accounting for such serial autocorrelation is very misleading and prone to false positives. Autocorrelation was modeled using autoregressive models as described in the Methods section. Based on the pattern of Figure 18, there was no linear trend. However, the three-year trends (2006-2007-2008 and 2008-2011-2013) were tested and both were found to be highly significant ($p<0.0005$).

Analogous models were developed for the remaining Salmon-Forever gaging stations (Figures 19-24) Partial residual plots were examined to determine the best linearizing logarithmic or power transformation for discharge and each API variable. For station FTR, a power transformation of discharge ($Q^{0.35}$) linearized the model better than log(Q), and the optimal API expression was $H88^{0.70}$. The selected bivariate sediment rating curve models for all stations are summarized in Table 8. None of the stations exhibited a significant increasing or decreasing linear trend over the period of record. Station KRW experienced a statistically significant dip in 2007 and 2008 ($p=0.0028$), much like SFM, with a return to the long-term average in 2011 and 2013. The KRW mean SSC for a given condition in 2008 was 22% below the long-term mean. The trends at stations FTR and HHB are both very flat for the entire monitoring period.

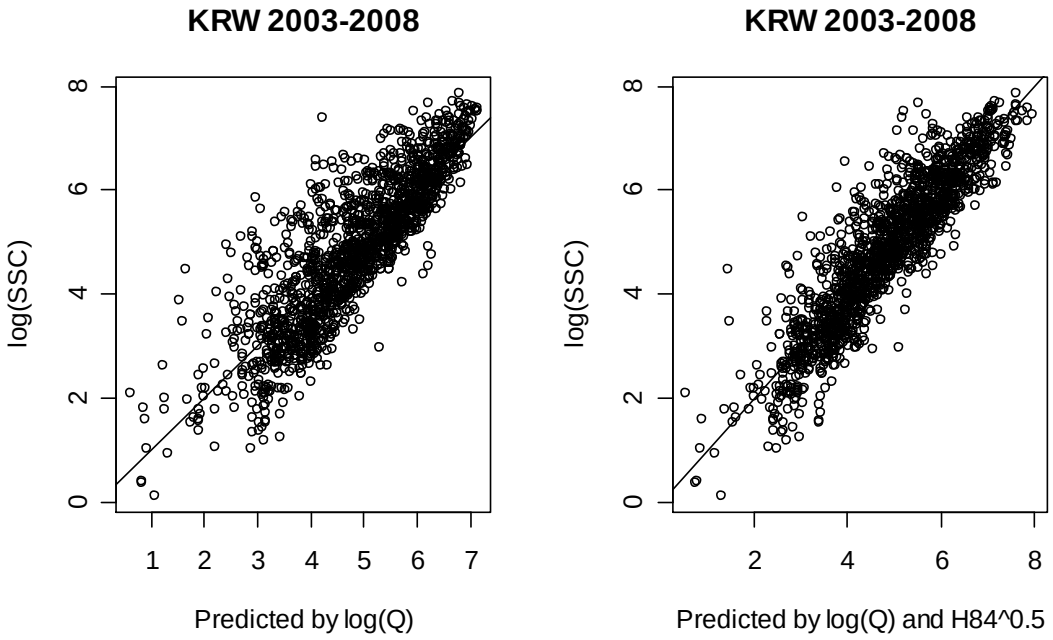

Figure 19. Observed versus predicted SSC from bivariate regression models predicting log(SSC) at station KRW as a linear function of (1) log(discharge) and (2) log(discharge) and hourly API ($H84^{0.5}$). Adding API to the model increased R^2 from 0.729 to 0.817.

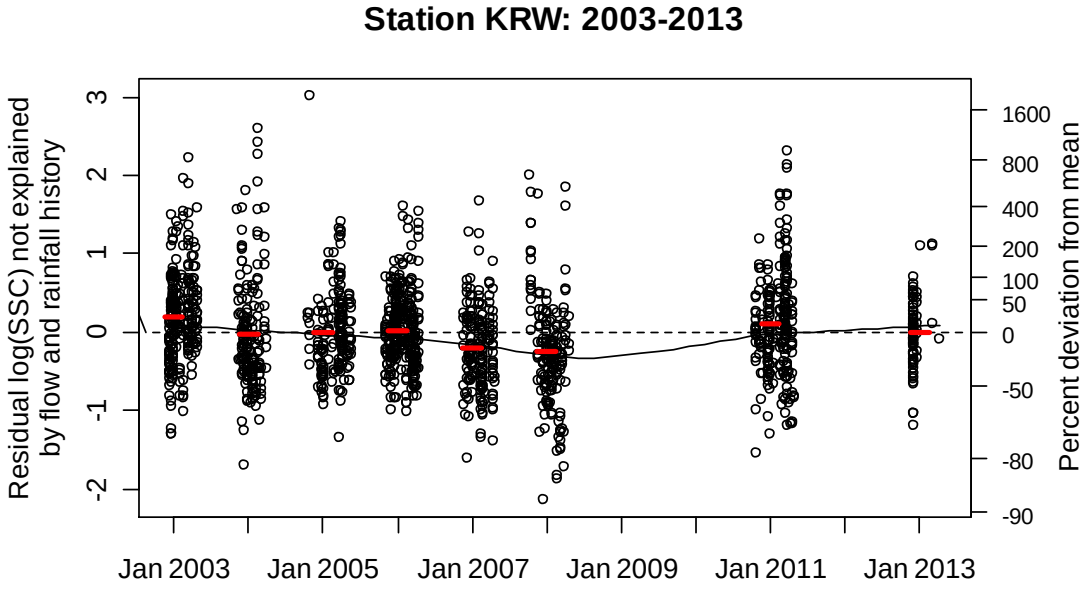

Figure 20. Sequence of residuals from bivariate regression model predicting log(SSC) at station KRW as a linear function of log(discharge) and hourly API ($H84^{0.5}$). Curve is fit by loess, with smoothing parameter = 0.67. Red bars show annual means.

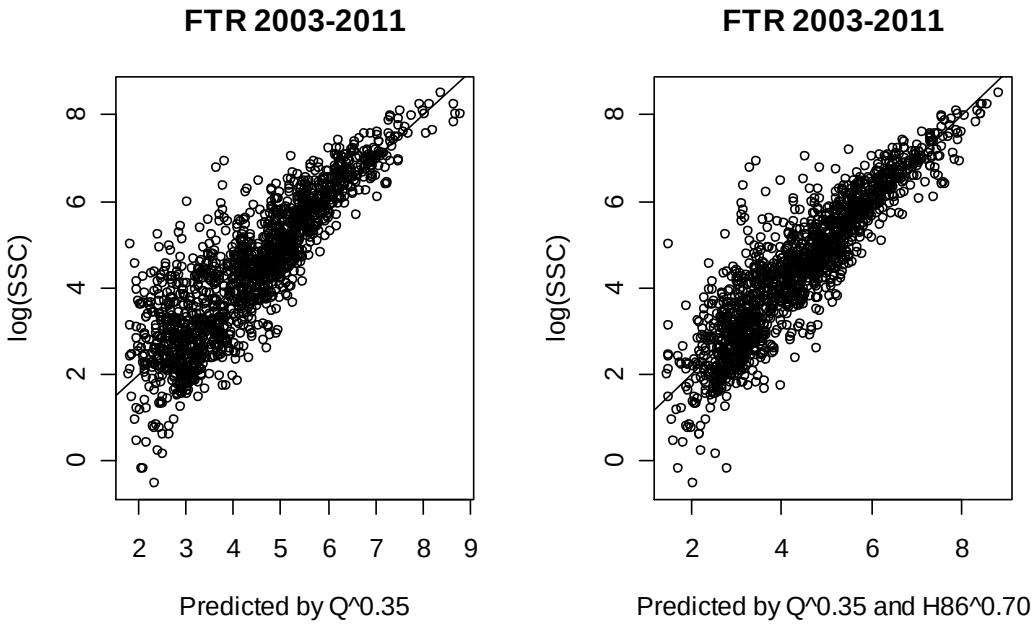

Figure 21. Observed versus predicted SSC from bivariate regression models predicting log(SSC) at station FTR as a linear function of (1) discharge ($Q^{0.35}$) and (2) discharge ($Q^{0.35}$) and hourly API ($H86^{0.7}$). Adding API to the model increased R^2 from 0.747 to 0.810.

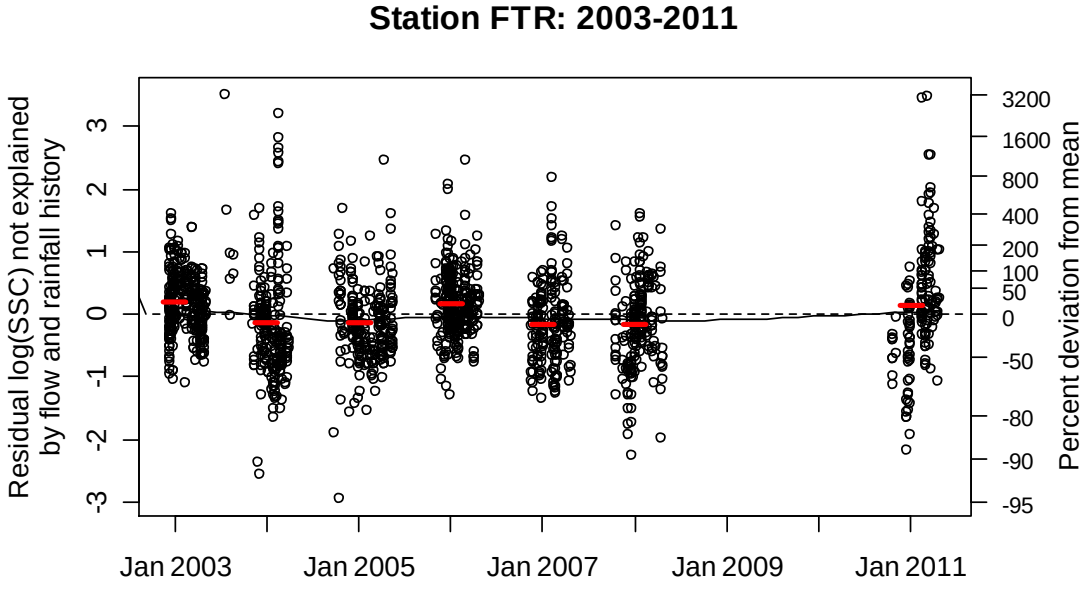

Figure 22. Sequence of residuals from bivariate regression model predicting log(SSC) at station FTR as a linear function discharge ($Q^{0.35}$) and hourly API ($H88^{0.7}$). Curve is fit by loess, with smoothing parameter = 0.67. Red bars show annual means.

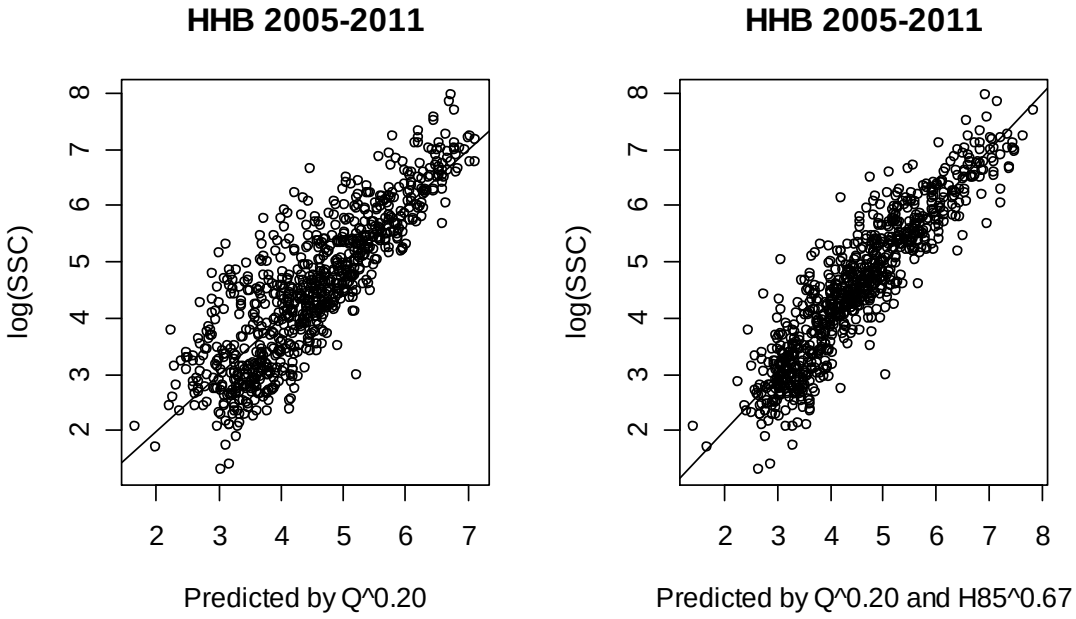

Figure 23. Observed versus predicted SSC from bivariate regression models predicting log(SSC) at station HHB as a linear function of (1) discharge ($Q^{0.20}$) and (2) discharge ($Q^{0.20}$) and hourly API ($H85^{0.67}$). Adding API to the model increased the adjusted R^2 from 0.709 to 0.830.

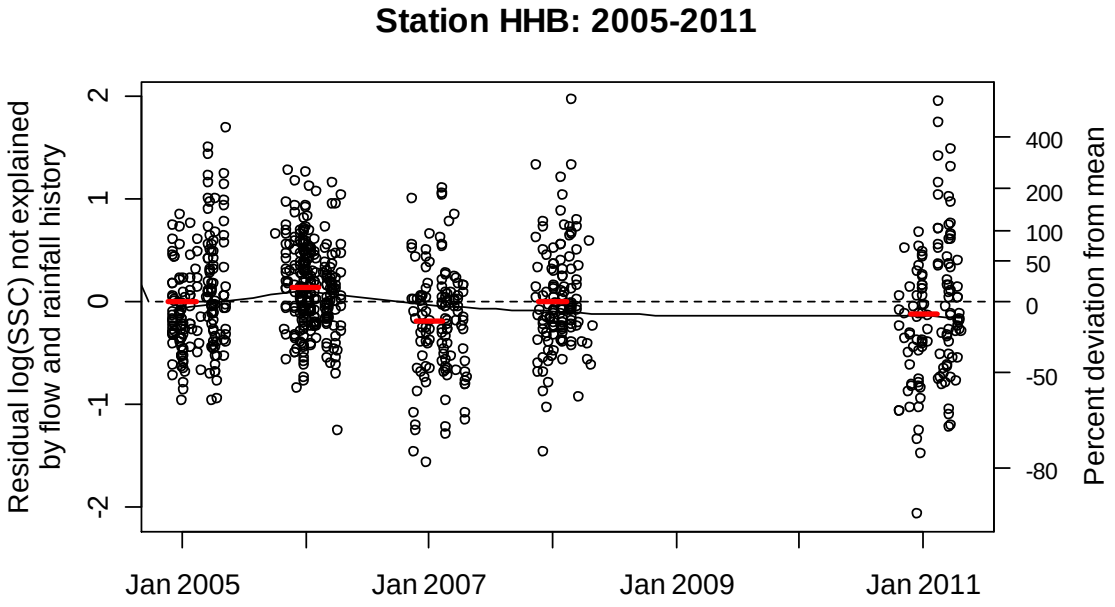

Figure 24. Sequence of residuals from bivariate regression model predicting log(SSC) at station HHB as a linear function discharge ($Q^{0.20}$) and hourly API ($H85^{0.67}$). Curve is fit by loess, with smoothing parameter = 0.67. Red bars show annual means.

Relative Trends in Storm Event Mean SSC

The response variable in these models is the ratio of storm event load to storm event flow, scale by a constant to represent SSC in mg/L. Figures 25-28 show the regressions and residuals trends. Mean SSC at KRW appears to have gradually declined relative to SFM (p=0.026). Both KRW and SFM declined relative to FTR in 2006-2008 (p<0.005). Those trends seem to have ended or reversed by 2011. If we assume SSC at FTR is unchanging, as the analysis in the previous section suggests, then the patterns at KRW and SFM are consistent with the 2006-2008 dips seen in Figures 18 and 20. The 2005-2008 decline at HHB is statistically weaker (Table 9) and not supported by Figure 24.

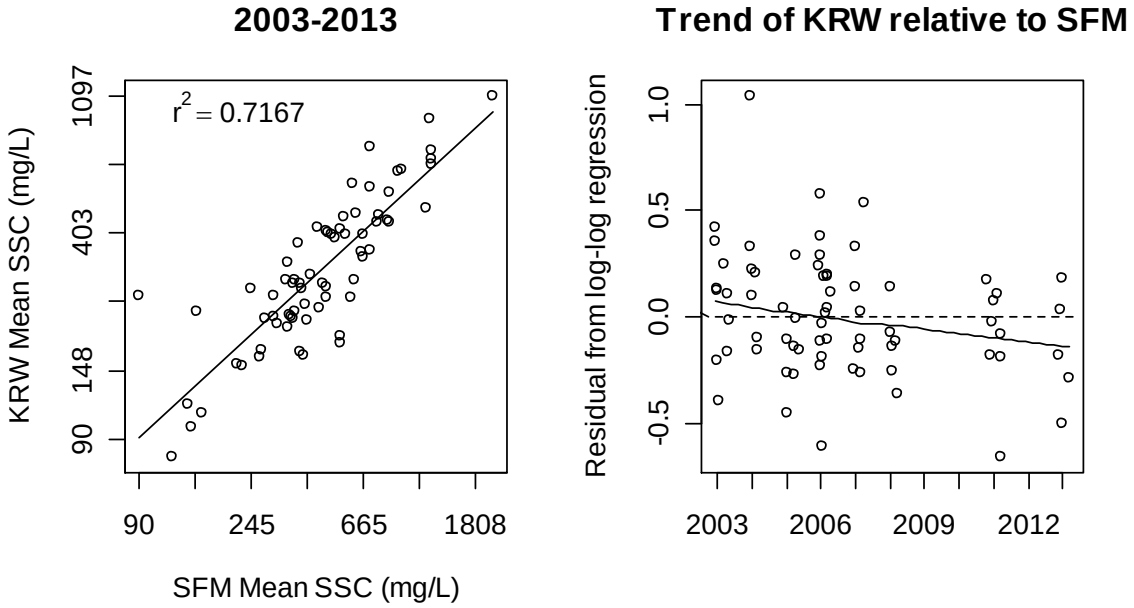

Figure 25. Trend analysis of storm event mean SSC at KRW relative to SFM. Both variables were transformed by logarithms.

Table 9. Summary of relative trends in storm event mean SSC

Y variable	X variable	Years	Trend?	R^2	Error model	Trend p-value
log(KRW)	log(SFM)	2003-2013	decreasing	0.7167	IID	0.0262
$KRW^{0.5}$	$FTR^{0.5}$	2003-2011	nonlinear?	0.6866	IID	0.3278
		2003-2008	decreasing	0.7171	AR(1)	0.0914
		2006-2008	decreasing	0.7134	IID	0.0014
log(SFM)	log(FTR)	2003-2011	nonlinear?	0.4006	IID	0.766
		2006-2008	decreasing	0.4595	IID	0.0023
log(HHB)	log(FTR)	2005-2011	nonlinear	0.8772	none	no test
		2005-2008	decreasing	0.8836	IID	0.0216

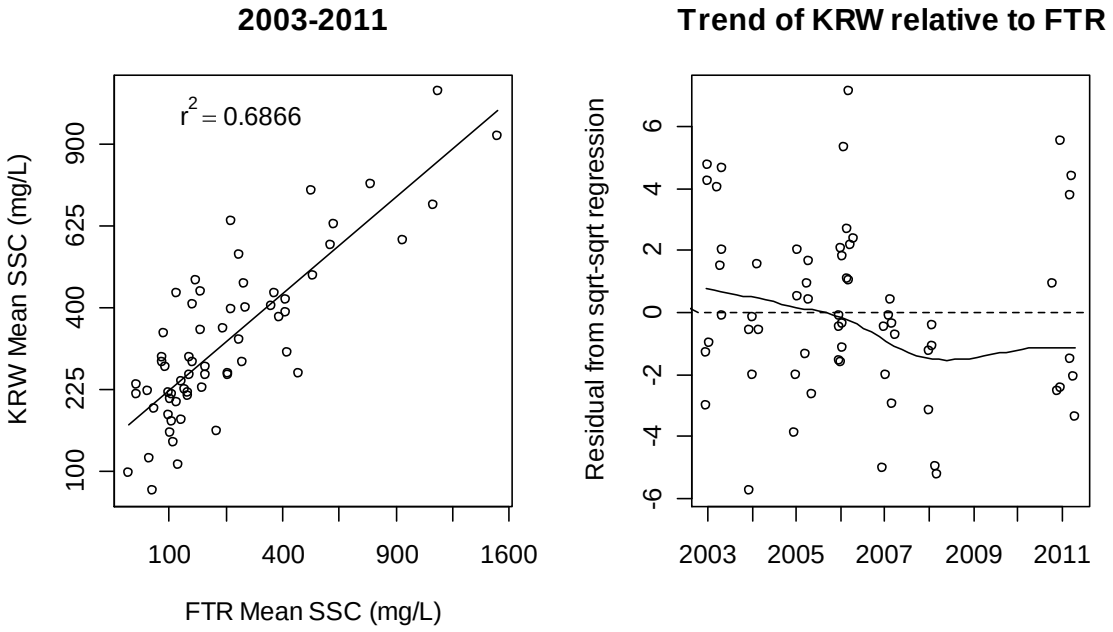

Figure 26. Trend analysis of storm event mean SSC at KRW relative to FTR. Both variables were transformed by square roots.

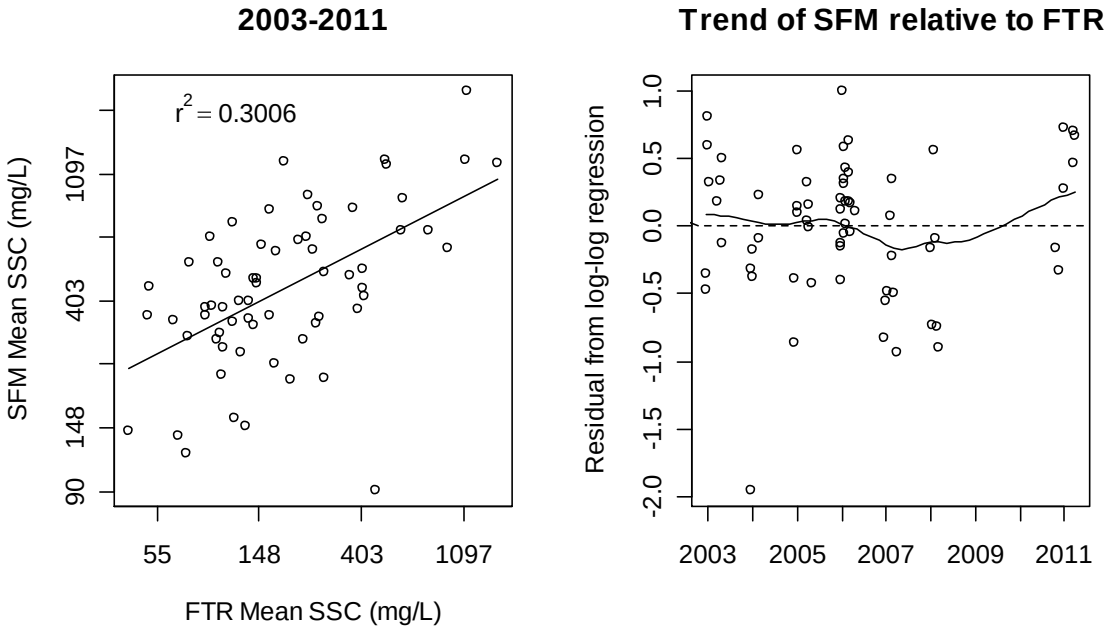

Figure 27. Trend analysis storm event mean SSC at SFM relative to FTR. Both variables were transformed by logarithms. For statistical analyses, the outlier at the bottom was omitted, raising the r^2 to 0.4006.

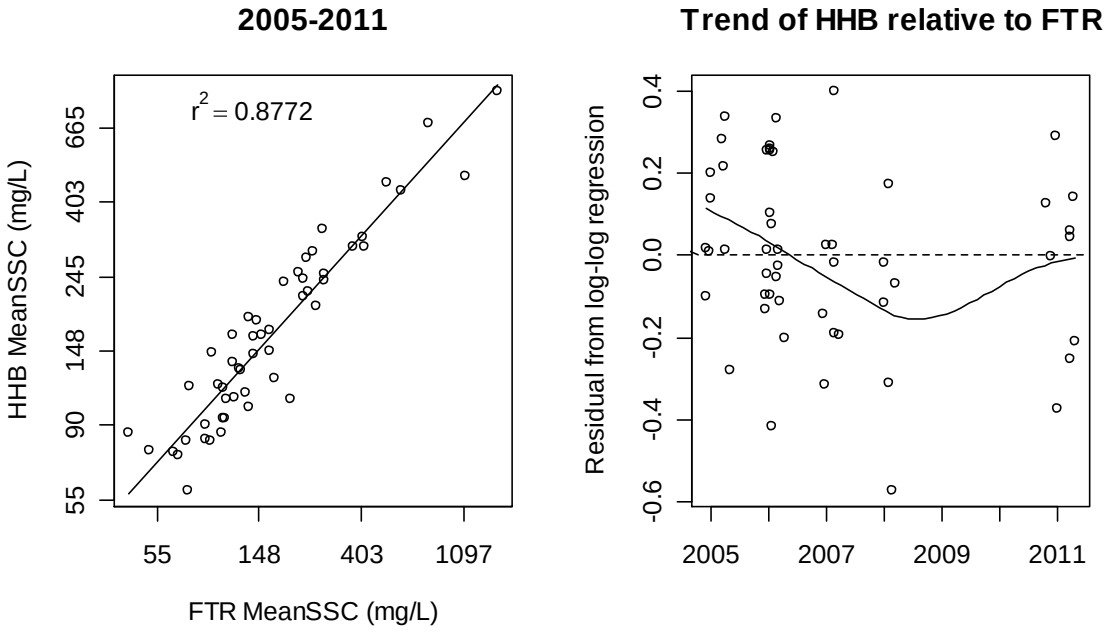

Figure 28. Trend analysis of storm event mean SSC at HHB relative to FTR. Both variables were transformed by logarithms.

Models for Storm Event Loads using Event Flows and Peaks

Storm event loads were modeled as a function of event flows and peaks. The logarithm or square root of these predictors are highly explanatory of event load, both individually and in combination. Transformations were selected based on examination of partial residual plots. In all cases both variables were highly significant in bivariate regressions for the logarithm of event load. Serial autocorrelation was detected in the residuals of models for SFM and FTR, and autoregressive models were incorporated into the models for testing trends. There was not a significant linear trend for any of the stations (Table 10). However, scatterplots (Figures 29-32) of the residuals from the model (before adding the time variable), suggest trends during shorter periods within the record. Several of these trends were tested using the same method as for the entire period (Table 10). Because the periods tested were suggested by the plots, the p-values for sub-periods should be taken as relative measures only. The most significant of these sub-trends is the 2006-2008 dip at KRW, uptrends from 2008-2013 at SFM and KRW, and the decline from 2006-2011 at HHB. Evidence supporting the other trends is weak.

Table 10. Best bivariate models for logarithm of storm event load, and tests for overall linear trend. The direction of trend, if any, is indicated by +/- after the p-value. Adjusted R^2 is before adding the time variable.

Station	Years	Flow variable	Peak variable	Adjusted R^2	Error model	trend p-value
SFM	2003-2013	log(flow)	log(peak)	0.8686	AR(2)	0.2045
	2003-2008	log(flow)	log(peak)	0.8577	AR(2)	0.0211-
	2006-2008	log(flow)	log(peak)	0.8837	CAR1	0.3569
	2008-2013	log(flow)	log(peak)	0.8806	IID	0.0027++
KRW	2003-2013	$flow^{0.5}$	$peak^{0.5}$	0.8772	AR(3)	0.6798
	2003-2008	$flow^{0.5}$	$peak^{0.5}$	0.8526	AR(2)	0.0211-
	2006-2008	$flow^{0.5}$	$peak^{0.5}$	0.9577	IID	0.0004--
	2008-2013	$flow^{0.5}$	$peak^{0.5}$	0.9203	IID	0.0071+
FTR	2003-2011	log(flow)	log(peak)	0.9212	AR(1)	0.3154
	2003-2007	log(flow)	log(peak)	0.9381	IID	0.0390-
HHB	2005-2011	$flow^{0.5}$	$peak^{0.5}$	0.9203	IID	0.0602
	2006-2011	$flow^{0.5}$	$peak^{0.5}$	0.9246	IID	0.0086-

CAR1 = order 1 continuous time autocorrelation structure (Pinheiro and Bates, 2000)
AR(n) = autogressive process of order n.
IID= independently and identically distributed

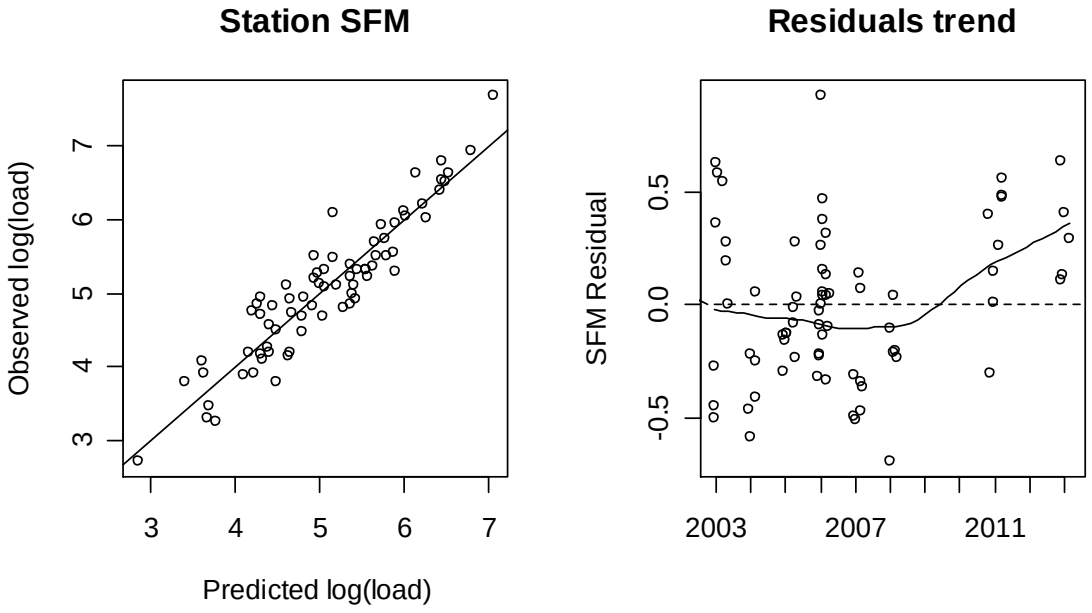

Figure 29. Model fit and trend for storm event loads at station SFM

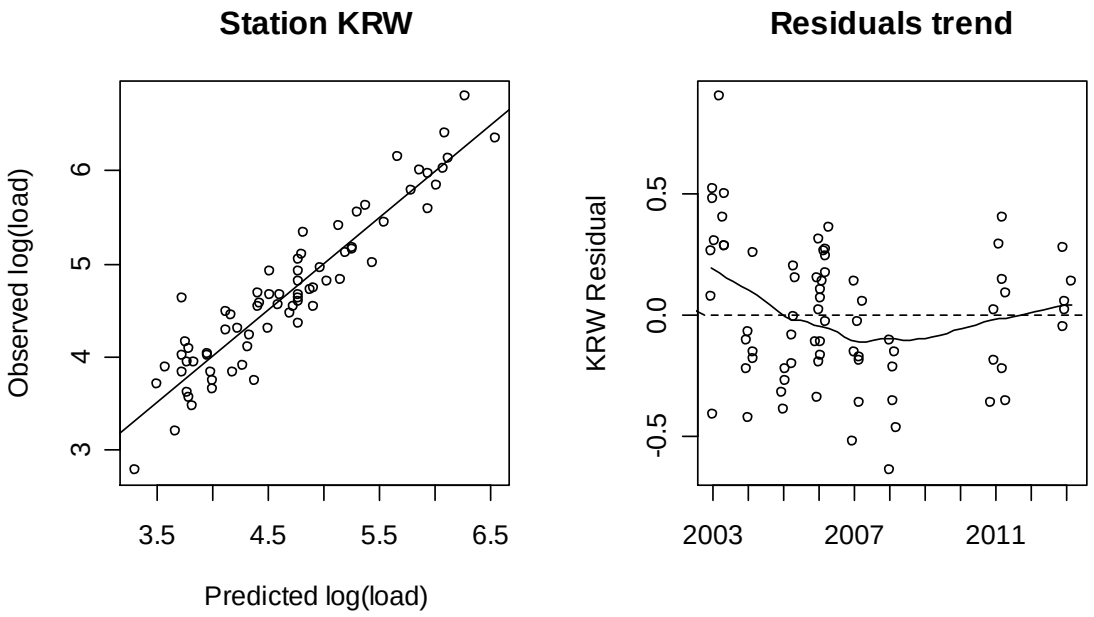

Figure 30. Model fit and trend for storm event loads at station KRW

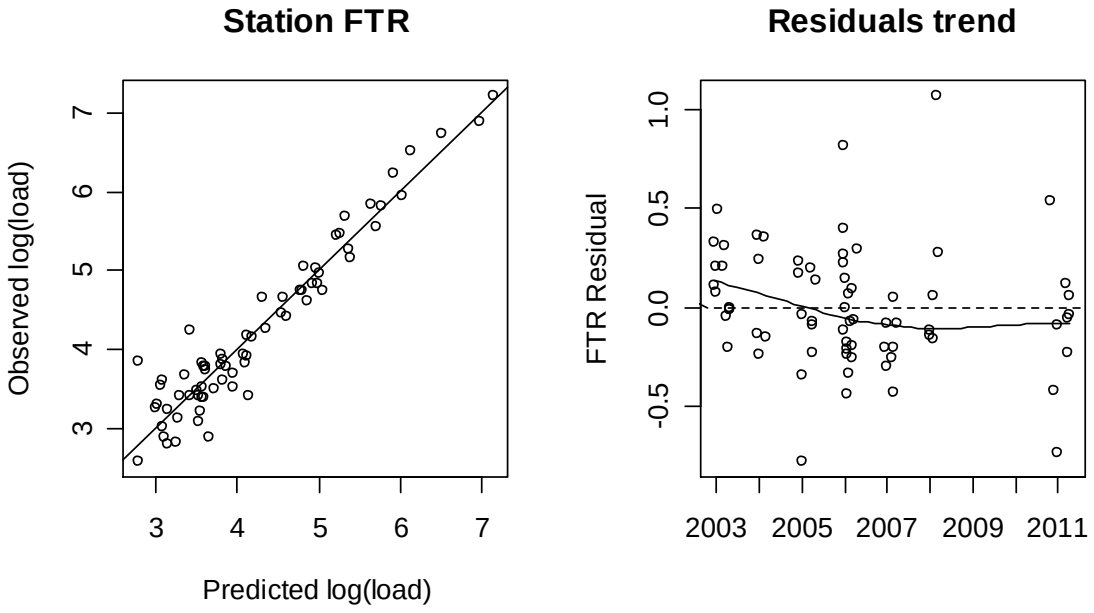

Figure 31. Model fit and trend for storm event loads at station FTR

Figure 32. Model fit and trend for storm event loads at station HHB

Relative Trends in Storm Event Loads

Figures 33-36 show the regressions comparing storm event loads between stations alongside plots depicting trends in associated residuals. Despite strong relationships between KRW and SFM loads (R^2=0.846) and between FTR and HHB loads (R^2=0.913), no significant trends were found relating storm event loads between watersheds within or across basins (Table 11).

Table 11. Summary of relative trends in storm event load

Y variable	X variable	Years	Trend?	R^2	Error model	Trend p-value
log(KRW)	log(SFM)	2003-2013	flattish	0.8461	IID	0.3583
		2007-2013	decreasing	0.8991	IID	0.1174
$KRW^{0.5}$	$FTR^{0.5}$	2003-2011	flat	0.7941	IID	0.3090
		2003-2008	flat	0.8207	IID	0.7370
		2006-2008	declining	0.8133	IID	0.0647
log(SFM)	log(FTR)	2003-2011	nonlinear?	0.5231	IID	0.9393
		2006-2008	declining	0.5244	AR(1)	0.1249
		2007-2011	rising	0.6186	IID	0.0649
log(HHB)	log(FTR)	2005-2011	flattish	0.9127	IID	0.6206
		2005-2008	declining	0.9131	IID	0.3612
		2007-2011	rising	0.8843	IID	0.299

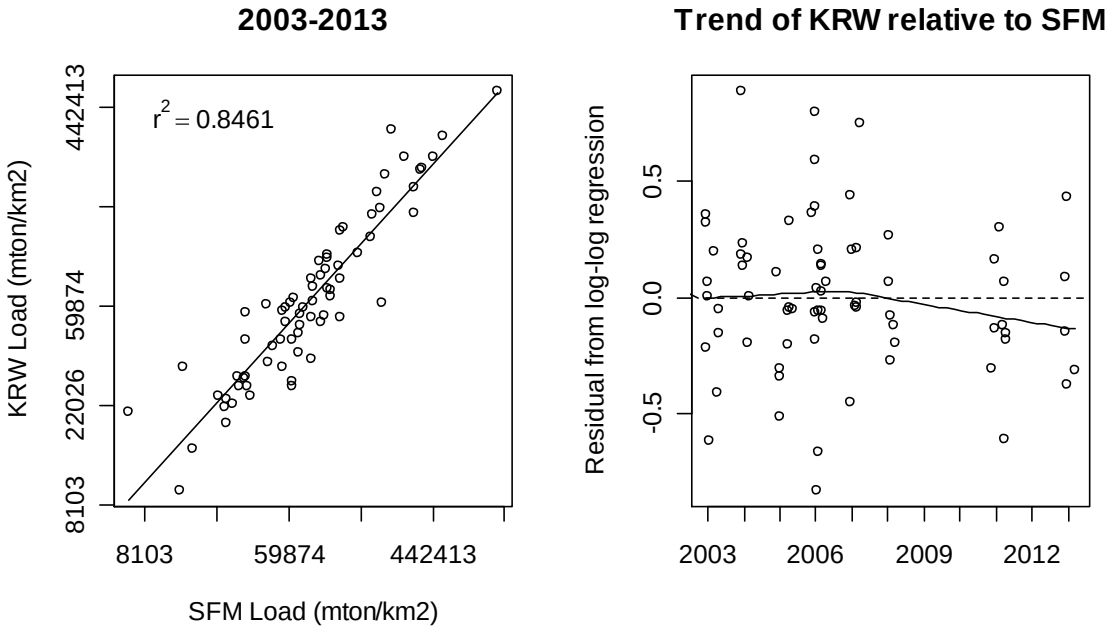

Figure 33. Trend analysis of storm event load at KRW relative to SFM. Both variables were transformed by logarithms.

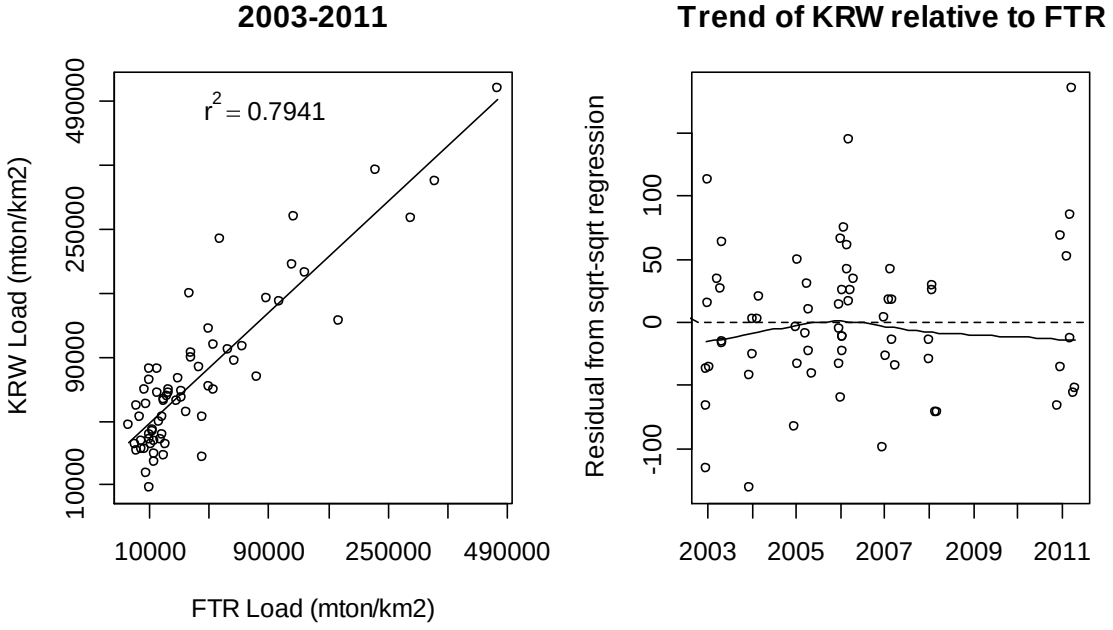

Figure 34. Trend analysis of storm event load at KRW relative to FTR. Both variables were transformed by square roots.

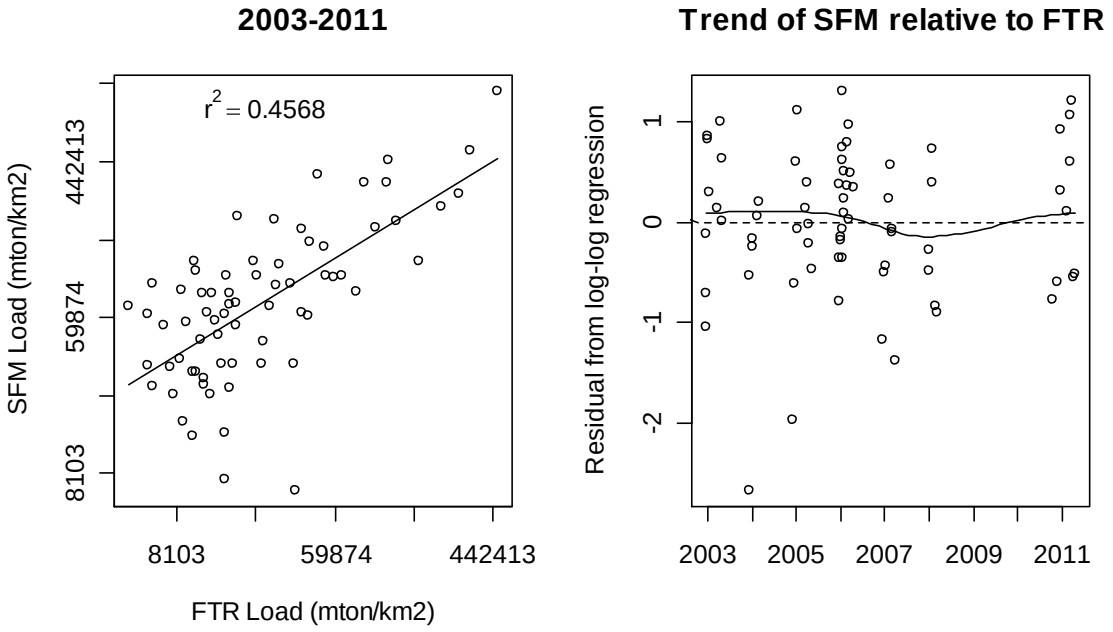

Figure 35. Trend analysis storm event load at SFM relative to FTR. Both variables were transformed by logarithms. For statistical analyses, the lowest outlier at the bottom was dropped, raising the r^2 to 0.5231.

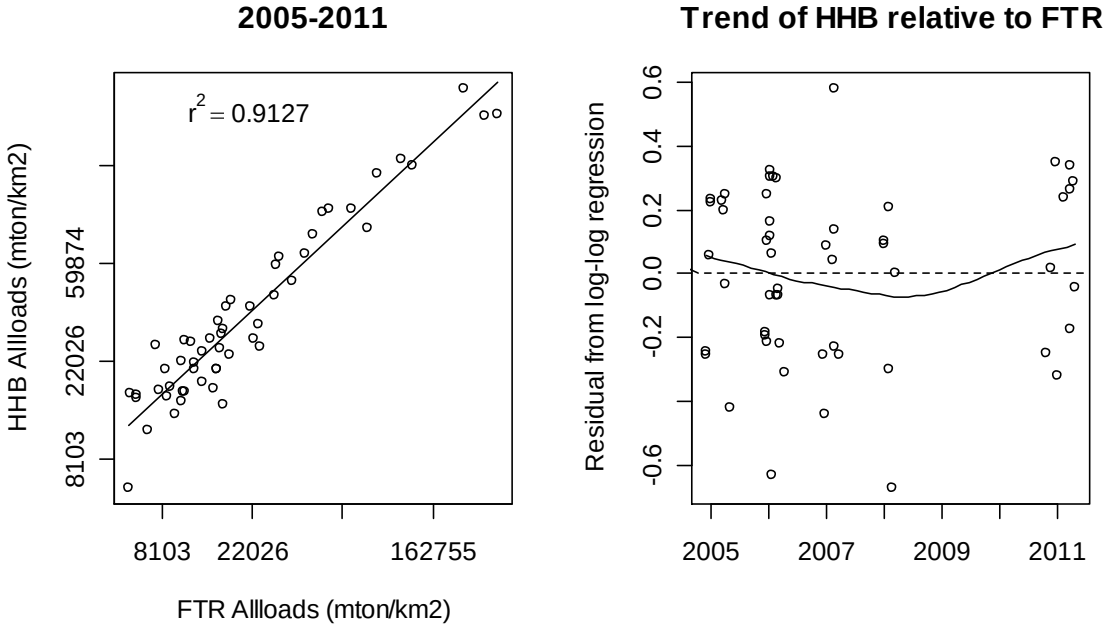

Figure 36. Trend analysis of storm event load at HHB relative to FTR. Both variables were transformed by logarithms.

Mixed Effects Models for Storm Event Load

The stations can be combined into a single model for storm event load, and this increases the power for trend detection. Sullivan et. al. (2013) took this approach with annual loads (not storm event loads) using annual peak flow and year as predictors. They did separate analyses on "event" (wet) years, and "non-event" (dry) years, and found that loads trended downward with year. Proper application of the technique requires accounting for spatial or temporal correlation. If many nearby or nested stations are combined, spatial autocorrelation is likely to be important. In storm event models, temporal autocorrelation may be important.

Storm event loads were modeled using event flows and peaks in a mixed-effects model including autocorrelated errors. This model is similar to that described in the previous section *Models for Storm Event Loads using Event Flows and Peaks*, but all stations are combined into one model and station is treated as a random effect to account for the lack of independence that arises because observations at any given station resemble each other more than those from different stations. For example, for each station, a deviation in the coefficient of one of the predictor variables could be modeled as a random effect. As a random effect, only the variance of the deviation needs to be estimated. If station were instead modeled as fixed effect, a coefficient would be estimated for each station.

Loads, flows, and peaks were all log-transformed, and error was modelled as an order 2 autoregressive process. The time variable, as in the analyses above, was the date at the start of the event. The only random effect that improved the model was a constant associated with each station. A linear trend was not significant in models for 2003-2008 ($p=0.125$), 2003-2011 ($p=0.296$), or 2003-2013 ($p= 0.594$). If the autocorrelated error were ignored, the trend for 2003-2008 would be judged significant ($p=0.0013$). Figure 37 shows the trend in residuals from the mixed effects model for 2003-2013.

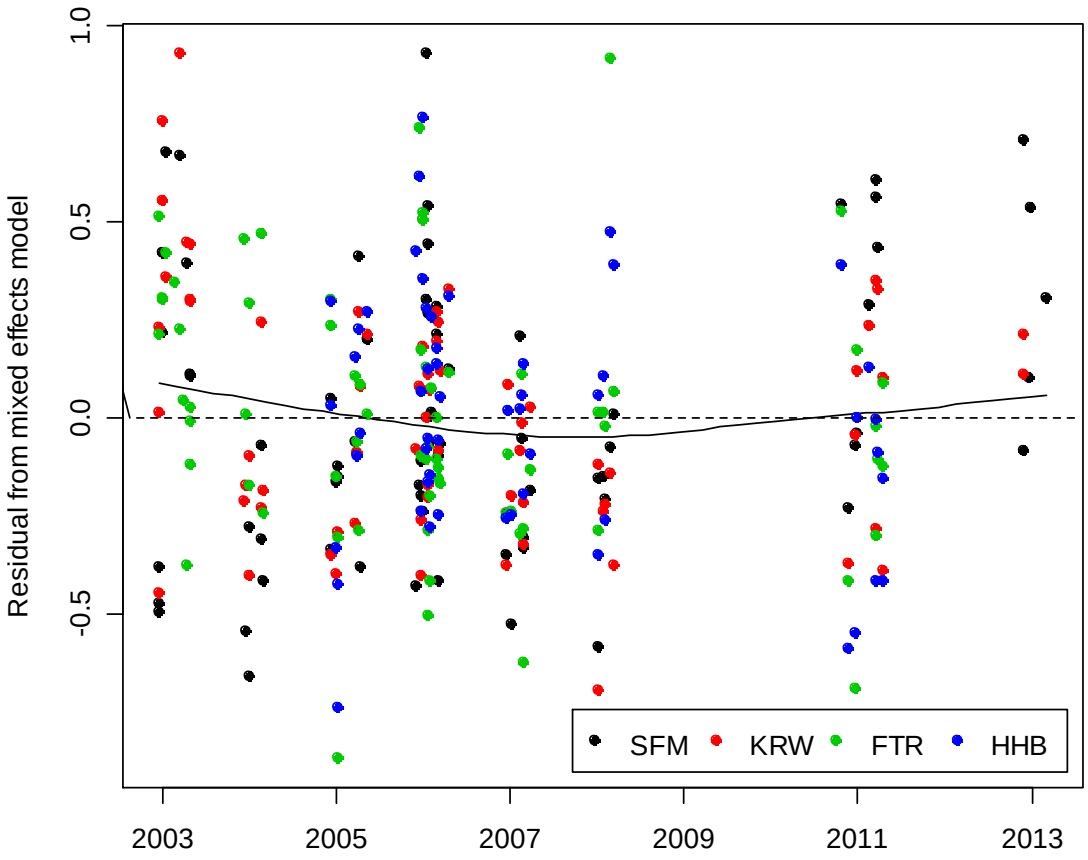

Figure 37. Trend for storm event loads at all stations combined based on mixed effects model accounting for flow volume and peak magnitude.

The analogous model for annual sediment loads using *annual* flows, peaks, and water year as predictors does not have temporally correlated errors. Water year was significant ($p=0.0083$) as a linear effect. The result mirrors what Sullivan et al. (2013) found with their analogous mixed model, based on HRC gaging stations in Elk River and Freshwater Creek. However, the pattern in the residuals does not appear to be linear (Figure 38) at least at SFM and KRW. Differences in trend among stations are difficult to discern because of the small number of data points and wide scatter. As a result, a random effect of station on time, if present, is unlikely to be detected statistically, lending false confidence in the notion of a common trend. The higher resolution storm event models provide a more comprehensive view of trends for each watershed.

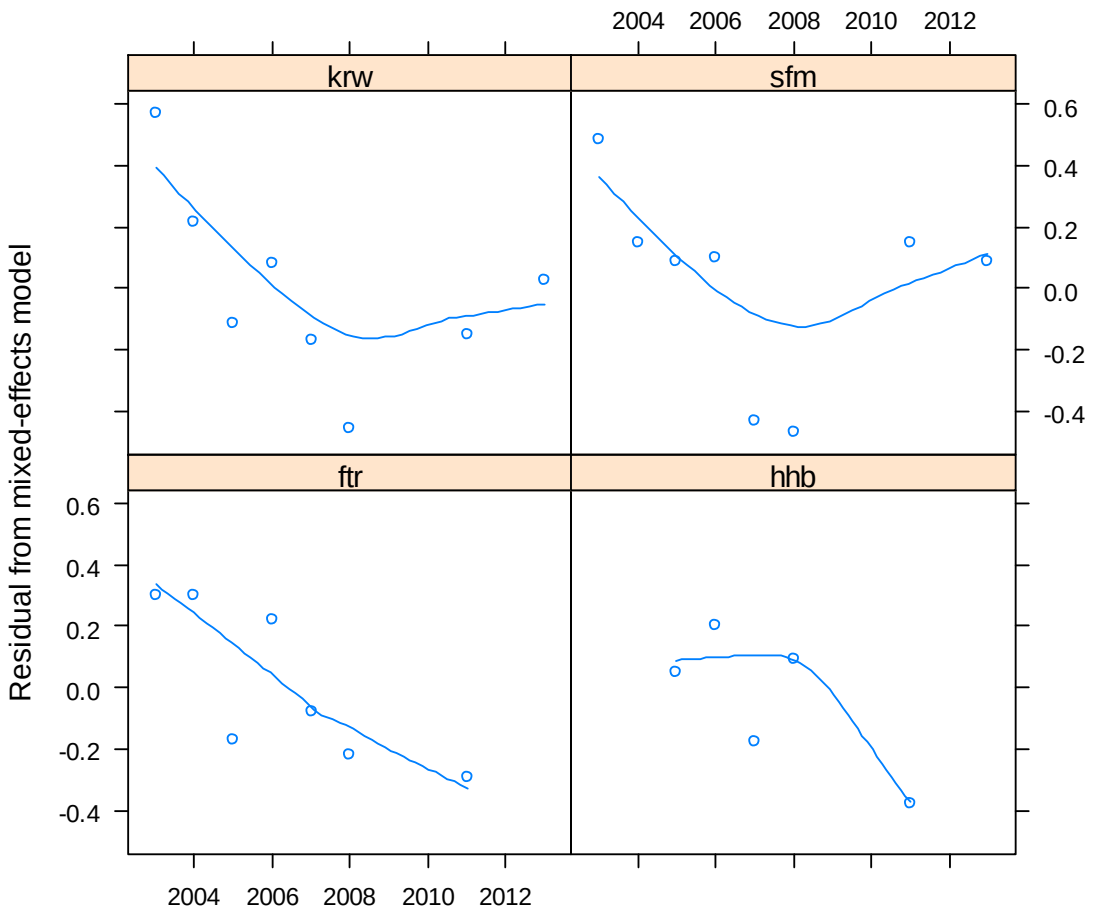

Figure 38. Trend for annual loads at all stations based on mixed effects model accounting for flow volume and peak magnitude.

DISCUSSION AND INTERPRETATION

Peak flows

Models for storm peak flow based on rainfall were subject to moderately high variability, with adjusted multiple R^2 varying between 0.43 and 0.58. Analysis of residuals suggested an increase of about 25% in 6-hr peak flow during the monitoring period at station HHB, for fixed antecedent rainfall conditions. An increase was also seen relative to peaks at station FTR. A change of this magnitude in peak flows seems quite unlikely absent a major reduction in vegetation in the watershed. Harvesting in Freshwater Creek between 2004 and 2012 totaled 26% of the watershed area, or an equivalent clearcut area of about 19% (Table 12). According to Figure 14 of the Water Board's Empirical Peak Flow Reduction Model, based on the peaks model developed for Caspar Creek (Lewis et.

al, 2001), this rate of harvest spread over a decade was expected to reduce peak flows over conditions that existed at the time.

The HH2 cross-section, immediately downstream of the bridge where discharge is gaged at HHB, showed aggradation of 42 ft^2 between 2000 and 2010, or about 12% of the bankfull cross-section area (stage 10 ft). Vertical aggradation averaged 0.43 ft. The average 6-hr peak at HHB was 542 cfs, or a stage of roughly 6 ft. It is unknown whether the aggradation occurred after gaging was begun in 2005, but if the stage at that discharge increased after 2005 by the same 0.43 ft as the total aggradation that occurred, the rating equation would predict a discharge that is 14% higher. Only one discharge measurement has been made at the gaging station since HY2008, at a stage of 4.78 ft, and it conformed well to the existing rating equation (Figure 4); it was not displaced to the right. Although the rating equation was modified, the change was trivial. So it seems unlikely that the apparent increase in peak flows can be explained by aggradation, and the change is greater than expected from forest harvesting. It is possible that additional aggradation has affected the rating curve since the last cross-section measurement was made in September 2010, although that would not explain the changes that were already visible in HY2010. It seems likely that the majority of the increase is an artifact of aggradation at the station.

Peak flow increases were detected at KRW from 2003 to 2006, when compared to SFM and FTR (Figures 11-12). But these changes are not mirrored in the analysis of peak flows based on rainfall. KRW does not show an increase in that period, and SFM and FTR do not show a decrease for given rainfall conditions (Figures 7-9). Aggradation was measured at both stations SFM (0.57 ft) and KRW (0.56 ft) between 2002 and 2006, so the KRW change relative to FTR could be indicative of a change in stage for a given discharge, but that explanation would be less likely for the change relative to SFM. Only one rating curve has been used at KRW (Figure 2) and it is based on measurements taken primarily from 2001 to 2005. Whatever changes in peak flows may have taken place before 2006, none of the analyses point to a continuation of the trends beyond 2006.

Sediment

If changes in the stage-discharge rating curves have affected flow estimates, then analyses of sediment loads need to be interpreted with caution. Each type of analysis is considered here with respect to the potential confounding of results.

1. **Modeling of SSC based on discharge and API**. Since discharge is one of the predictor variables, to the extent that discharge contains false trends, it could lead to detection of false trends of opposite sign in SSC. For example, one might expect to see a downtrend in SSC at HHB for the years 2009-2013, or at KRW from 2003-2006. No such trend was seen at HHB or KRW.
2. **Modeling of storm event loads on storm peaks and storm flows**. Discharge is in both predictors and the response. An error in the rating equation will bias all these variables in the same direction. Therefore this analysis is relatively robust to errors in rating equations.

3. **Relative trends in event mean SSC**. Mean SSC is the quotient of event load and flow volume. An error in the rating equation will bias both numerator and denominator in the same direction. Mean SSC will not be free of bias, but this analysis should be relatively robust to errors in rating equations.
4. **Relative trends in event loads**. Since event loads are computed from discharge and SSC, event loads will be biased by errors in rating equations. Therefore if discharge contains false trends, one would expect to see similar trends in SSC. However, no trends at all were detected among event loads at different gaging stations.

Models for sediment concentration using instantaneous discharge and an hourly API had fairly high predictive value with adjusted R^2 in the range of 0.70 to 0.83. No decade-long trends were found. The pattern of unexplained variation was very flat at both FTR and HHB. However, both SFM and KRW experienced significant downward trends from 2006 to 2008, followed by a return to the long term mean in 2011. Station SFM was 35% above the long term mean in 2013. Relative trends in storm event mean SSC also suggested declines at SFM and KRW from 2006 to 2008 followed by a return to normal in 2011. However these stations could not be compared to FTR in 2013, since the FTR data are not yet available. Mean SSC at KRW also may have declined somewhat relative to SFM over the 11-year monitoring period but the trend is barely significant.

Models for storm event loads using peaks and flows were quite strong with adjusted R^2 in the range of 0.85 to 0.94 and sample sizes from 54 to 76. There was no evidence of decade-long trends, using either station-specific models or a mixed-effects model combining all stations. The most significant shorter-duration trends were the decline at KRW from 2006 to 2008 and increases at both KRW and SFM from 2008 to 2013. These results parallel those from the analysis of mean SSC.

There was also a downtrend in storm event loads detected (using peaks and flows) at station HHB between 2006 and 2011, which goes opposite of the expected trend based on peak flows. Therefore concentrations must have declined. In corroboration of that expectation, the event mean SSC was found to decline at HHB relative to FTR from 2005 to 2008. No trend was found in instantaneous SSC, controlling for discharge and API. But a false decline in discharge caused by aggradation would have given rise to an apparent increase in SSC using that model; that effect may well have erased the signal of declining SSC expected on the basis of results for event loads and event mean SSC.

The harvested acreages in Elk River and Freshwater Creek watersheds are presented in Table 12 for comparison with the trend results. Areas were converted roughly to equivalent clearcut acres using factors of 0.9 in 2006-7, 0.75 in 2008, and 0.6 in 2009-2012 proposed by Adona White (personal communcation), based on the transfer of management from Palco to HRC in 2008. Former practices of primarily clearcutting with selectively cut buffers have been replaced with group selection harvests limited to 50% of plan areas. The sediment concentrations and loads at SFM and KRW reversed their declines following the summer of 2010 which was one of the heaviest years of harvesting (Table 12) in both the North and South Fork of Elk River. The only bigger recent harvest

year in the South Fork may have been 2012 (only the proposed acreage is known), and that harvest was followed by another sediment increase in 2013. Notably, however, an even larger portion of the HHB watershed was harvested in 2010, where there was no uptick detected the following winter.

Table 12. Percentages of watersheds harvested. Derived from data supplied by Adona White (North Coast Regional Water Quality Control Board). Values for 2012 are as proposed before completion. HHB 2001-2005 values were obtained from Randy Klein.

	Percent of area harvested			Percent equivalent clearcut area		
Year	KRW	SFM	HHB	KRW	SFM	HHB
2001	0.00	0.00	10.15	0.53	0.00	7.86
2002	4.93	3.06	3.27	2.18	0.82	2.96
2003	0.71	0.00	2.71	1.04	0.00	2.40
2004	2.70	0.99	3.71	0.38	0.00	3.47
2005	1.55	0.00	2.79	0.00	0.00	2.55
2006	1.33	1.46	1.58	1.19	1.32	1.43
2007	1.81	0.91	1.37	1.63	0.82	1.23
2008	1.57	1.51	2.09	1.17	1.14	1.56
2009	0.40	1.05	3.40	0.24	0.63	2.04
2010	2.87	3.40	3.90	1.72	2.04	2.34
2011	0.90	2.23	3.18	0.54	1.34	1.91
2012	2.30	3.71	3.73	1.38	2.23	2.24
Totals	21.07	18.33	31.99	12.01	10.33	41.87

SUMMARY

The main findings of this report are:

- Despite protection of 30% of the South Fork Elk watershed in the Headwaters Reserve, suspended sediment continues to discharge from SFM at substantially higher rates than the North Fork or Humboldt Bay gaging stations on Freshwater Creek and Jacoby Creek. Based on sediment yields measured in the Headwaters Reserve, average yields from lands managed for timber production in the South Fork probably exceed 370 mT/km^2, greater than the maximum annual yield measured at North Fork Elk, Freshwater Creek, or Jacoby Creek.

- Aggradation in lower Elk River has continued in the past decade and is widespread at often exceeding 1 ft in elevation or 100 ft2 in cross-sectional area per decade. The mean decadal rate of infill is greatest in the South Fork (92 ft^2), followed by the North Fork (65 ft^2) and lastly the main stem (54 ft^2). In Freshwater Creek, we have less information, but most cross-sections surveyed seem stable. Rates of infill since 1999 appear to be 30-50% of those in the Elk River. The mean decadal rate of infill for all cross-sections in Freshwater Creek has been 22 ft^2 in area and 0.3 ft in elevation.

- No trends in storm peaks were detected except at Freshwater station HHB, where peaks apparently rose 25% between 2005 and 2013. This may be mostly an artifact of aggradation observed at the rated cross-section. Canopy removal at an average rate of 2.1% per year cannot by itself account for the change.

- Comparing pairs of stations, no relative trends in storm event loads were detected, but other methods did reveal trends.

- Elk River stations SFM and KRW saw declines in both storm event loads and instantaneous SSC (controlling for hydrologic conditions) from 2006 to 2008, followed by a bounce back to the mean in 2011. Instantaneous SSC at SFM jumped to 35% above the mean in 2013. These trends are supported by relative trends comparing event mean SSC between pairs of stations.

- At Freshwater station FTR all response variables were flat over the study period. No significant trends were detected.

- At the Freshwater station HHB, (controlling for hydrologic conditions), storm event loads trended downward in HY2006-2011, despite an apparent increase in flows. And event mean SSC declined relative to FTR in HY2005-2008.

REFERENCES

Achim Zeileis, T. Hothorn. 2002. Diagnostic Checking in Regression Relationships. R News 2(3), 7-10. URL http://CRAN.R-project.org/doc/Rnews/

Box, G.E.P. and G.M. Jenkins. 1970. Time Series Analysis, Forecasting, and Control. San Francisco: Holden Day.

Cleveland, W.S.; E. Grosse and W.M. Shyu. 1992. Local regression models. Chapter 8 of *Statistical Models in S* eds J.M. Chambers and T.J. Hastie, Wadsworth & Brooks/Cole.

Cook, R.D. and S. Weisberg. 1994. An Introduction to Regression Graphics. Wiley Series in Probability and Mathematical Statistics: New York. 253 p.

Durbin, J. and G.S. Watson. 1971. Testing for Serial Correlation in Least Squares Regression III. *Biometrika* **58**, 1–19.

Lewis, J., Keppeler, E., Ziemer, R.R., and S.R. Mori. 2001. Impacts of logging on storm peak flows, flow volumes and suspended sediment loads in Caspar Creek, California. In: Mark S. Wigmosta and Steven J. Burges (eds.) Land Use and Watersheds: Human Influence on Hydrology and Geomorphology in Urban and Forest Areas. Water Science and Application Volume 2, American Geophysical Union, Washington, D.C.; 85-125.

Lewis, J., R.E. Eads, and R.D. Klein. 2007. Comparisons of turbidity data collected with different instruments. Report on a cooperative agreement between the California Department of Forestry and Fire Protection and USDA Forest Service--Pacific Southwest Research Station (PSW Agreement # 06-CO-11272133-041); July 6, 2007.

Lewis, J. and R.E.Eads. 2009. Implementation Guide for Turbidity Threshold Sampling: Principles, Procedures, and Analysis. General Technical Report PSW-GTR-212, U.S. Department of Agriculture, Forest Service, Pacific Southwest Research Station.

Newcombe, C.P. and D. D. Macdonald. 1991. Effects of suspended sediments on aquatic ecosystems. North American Journal of Fisheries Management 11: 72-82.

Newcombe, C.P. and J.O.T. Jensen. 1996. Channel suspended sediment and fisheries: a synthesis for quantitative assessment of risk and impact. North American Journal of Fisheries Management 16: 693-727.

Pinheiro, J.C., and D.M. Bates. 2000. "Mixed-Effects Models in S and S-PLUS", Springer, esp. pp. 236, 243.

Pinheiro, J., D.M. Bates, S. DebRoy and D. Sarkar the R Core team. 2007. nlme: Linear and Nonlinear Mixed Effects Models. R package version 3.1-86.

R Development Core Team. 2008. R: A language and environment for statistical computing. R Foundation for Statistical Computing, Vienna, Austria. ISBN 3-900051-07-0, URL http://www.R-project.org.

Sakamoto, Y., M. Ishiguro, and G. Kitagawa. 1986. *Akaike Information Criterion Statistics*. D. Reidel Publishing Company.

Shumway, R.H. 1988. Applied Statistical Time Series Analysis. New Jersey: Prentice Hall. 379 pp.

Sullivan, K., D.M. Manthorne, R. Rossen, and A. Griffith. 2012. Trends in sediment-related water quality after a decade of forest management implementing an aquatic habitat conservation plan. Humboldt Redwood Company, Scotia, CA. 187 pp.